

561285

663

NASA CONTRACTOR
REPORT



NASA CR-12

NASA CR-12

PLANETARY AERONOMY

VI: ELECTRON TEMPERATURES IN THE IONOSPHERE

by A. Dalgarno, M. B. McElroy, and R. J. Moffett

Prepared under Contract No. NASw-395 by
GEOPHYSICS CORPORATION OF AMERICA
Bedford, Massachusetts
for

NATIONAL AERONAUTICS AND SPACE ADMINISTRATION • WASHINGTON, D. C. • SEPTEMBER 1963

CONTRACTOR REPORT CR-12

**PLANETARY AERONOMY VI:
ELECTRON TEMPERATURES IN THE IONOSPHERE
By A. Dalgarno, M. B. McElroy, and R. J. Moffett**

Prepared under Contract No. NASw-395 by
GEOPHYSICS CORPORATION OF AMERICA
Bedford, Massachusetts

for

NATIONAL AERONAUTICS AND SPACE ADMINISTRATION

CONTRACTOR REPORT CR-12

PLANETARY AERONOMY VI:
ELECTRON TEMPERATURES IN THE IONOSPHERE

By A. Dalgarno, M. B. McElroy, and R. J. Moffett
Geophysics Corporation of America
GCA Technical Report No. 62-11-N

ABSTRACT

Detailed calculations are described of the rate of heating of the ambient electrons arising from solar ultraviolet radiation and it is shown that the resulting difference between the electron temperature and the gas temperature at noon in a quiet ionosphere may reach a maximum value lying between 800° K and 1500° K at an altitude near 200 km but that the difference vanishes below about 120 km and above about 400 km. This is in accord with the analysis of the observational data by Bauer and Bourdeau which can therefore be explained as due to the direct action of solar ultraviolet radiation and it is unnecessary to postulate the existence of electric fields.

NATIONAL AERONAUTICS AND SPACE ADMINISTRATION

TABLE OF CONTENTS

<u>Section</u>	<u>Title</u>	<u>Page</u>
ABSTRACT		
LEGEND OF FIGURES		ii
1.	Introduction	1
2.	Production	2
	2.1 Model Atmospheres	2
	2.2 Solar Flux and Photoionization Rates	2
	2.3 Equilibrium Electron Densities	8
	2.4 Energy Distribution of Photoelectrons	8
3.	Energy Loss Processes	20
	3.1 Excitation and Ionization	20
	3.2 Excitation to Metastable States	21
	3.3 Vibrational Excitation of N ₂	25
	3.4 Rotational Excitation of N ₂	31
	3.5 Elastic Scattering by Neutral Particles and Positive Ions	34
	3.6 Elastic Scattering by Ambient Electrons	34
	3.7 Critical Altitudes and Energies	37
4.	Heat Flux and Cooling Processes	41
5.	Electron Temperatures	45
6.	Discussion	52
REFERENCES		54

LEGEND FOR FIGURES

- Figure 1. Noon total photoionization rates: Curve
(a) $T(\infty) = 1000^{\circ}\text{K}$
(b) $T(\infty) = 2000^{\circ}\text{K}$
(c) Watanabe and Hinteregger (1962).
- Figure 2. Noon photoionization rates for $T(\infty) = 1000^{\circ}\text{K}$ for O^+ , O_2^+ and N_2^+ .
- Figure 3. Noon photoionization rates for $T(\infty) = 2000^{\circ}\text{K}$ for O^+ , O_2^+ and N_2^+ .
- Figure 4. Distribution of photoelectrons produced by process
(1) for $T(\infty) = 1000^{\circ}\text{K}$.
- Figure 5. Distribution of photoelectrons produced by process (1)
for $T(\infty) = 2000^{\circ}\text{K}$.
- Figure 6. Total rate of deposition of photoelectron kinetic energy
(curve a) and of metastable energy (curve b) for
 $T(\infty) = 1000^{\circ}\text{K}$
- Figure 7. Total rate of deposition of photoelectron kinetic energy
(curve a) and of metastable energy (curve b) for
 $T(\infty) = 2000^{\circ}\text{K}$.
- Figure 8. Rates of energy loss to neutral particles (solid lines)
and to electrons (dashed line) for electrons of various
energies above 20 eV moving in the model atmosphere with
 $T(\infty) = 1000^{\circ}\text{K}$.
- Figure 9. Rates of energy loss to neutral particles (solid lines)
and to electrons (dashed line) for electrons of various
energies above 20 eV moving in the model atmosphere
with $T(\infty) = 2000^{\circ}\text{K}$.

Figure 10. Rates of energy loss to neutral particles (solid lines) and to electrons (dashed lines) for electrons of various energies below 20 eV moving in the model atmosphere with $T(\infty) = 1000^{\circ}\text{K}$.

Figure 11. Rates of energy loss to neutral particles (solid lines) and to electrons (dashed lines) for electrons of various energies below 20 eV moving in the model atmosphere with $T(\infty) = 2000^{\circ}\text{K}$.

Figure 12. Rates of energy loss through vibrational excitation of molecular nitrogen at unit density.

Figure 13. Rates of energy loss to neutral particles (solid lines) and to electrons (dashed lines) for electrons with energies between 1.5 eV and 4 eV moving in the model atmosphere with $T(\infty) = 1000^{\circ}\text{K}$.

Figure 14. Rates of energy loss to neutral particles and to electrons for electrons with energies between 1.5 eV and 4 eV moving in the model atmosphere with $T(\infty) = 2000^{\circ}\text{K}$.

Figure 15. Rates of energy loss through rotational excitation of N_2 (solid lines) and through elastic collisions (dashed lines) with the ambient electrons for $T(\infty) = 1000^{\circ}\text{K}$.

Figure 16. Rates of energy loss through rotational excitation of N_2 (solid lines) and through elastic collisions (dashed lines) with the ambient electrons for $T(\infty) = 2000^{\circ}\text{K}$.

Figure 17. Critical energies for the model atmosphere with $T(\infty) = 1000^{\circ}\text{K}$, assuming that the vibrational energy of N_2 is converted to thermal energy of (a) the neutral particles and (b) the electron gas.

Figure 18. Critical energies for the model atmosphere with $T(\infty) = 2000^{\circ}\text{K}$, assuming that vibrational energy of N_2 is converted to thermal energy of (a) the neutral particles and (b) the electron gas.

Figure 19. Heat fluxes to the ambient electrons for the atmosphere with $T(\infty) = 1000^{\circ}\text{K}$. curve (a) excluding metastable energy and excluding vibrational energy; curve (b) including metastable energy but excluding vibrational energy; curve (c) excluding metastable energy but including vibrational energy; curve (d) including metastable energy and including vibrational energy.

Figure 20. Heat fluxes to the ambient electrons for the atmosphere with $T(\infty) = 2000^{\circ}\text{K}$. The labelling of the four curves is as for Figure 19.

Figure 21. The right-hand side of Equation (24) as a function of T_e at an altitude of 400 km in the atmosphere with $T(\infty) = 1000^{\circ}\text{K}$.

Figure 22. Electron temperatures corresponding to the heat inputs of Figure 19.

Figure 23. Electron temperatures corresponding to the heat inputs of Figure 20.

ELECTRON TEMPERATURES IN THE IONOSPHERE

A. Dalgarno,
M. B. McElroy* and R. J. Moffett*

1. Introduction

Hanson and Johnson (1961) have suggested that energetic photoelectrons produced by the incident solar ultraviolet radiation may give rise to an electron temperature T_e in the daytime ionosphere which is higher than the neutral particle and positive ion temperature T_g and experimental evidence supporting this view has been obtained recently by Spencer, Brace and Carignan (1962) who find that T_e is much greater than T_g at altitudes between about 100 and 400 km, the maximum value of T_e lying between 2400°K and 3000°K . However, because the solar photon flux adopted by Hanson and Johnson is much less than that now observed (cf. Watanabe and Hinteregger 1962), because an important process--the electron impact excitation of vibrational levels of molecular nitrogen--was omitted from consideration, and because the significance of metastable energies as a source of heating was not investigated, the conclusions of Hanson and Johnson have only qualitative significance and a re-analysis is desirable.

*Department of Applied Mathematics, The Queen's University of Belfast,
Belfast, N. Ireland.

2. Production of Photoelectrons

2.1 Model Atmospheres

As model atmospheres we have selected two from those derived by Bates (1959) and Bates and Patterson (1961), one of which corresponds to a temperature of 1000°K at the base of the exosphere and the other to a temperature of 2000°K. The two models probably span the possible atmospheres. The associated number densities and temperatures are reproduced in Table 1.

2.2 Solar Flux and Photoionization Rates

For the incident flux of solar photons we have adopted the values quoted by Watanabe and Hinteregger (1962) and they are reproduced in Table 2. Using a model atmosphere which is roughly a mean of the two given in Table 1, Watanabe and Hinteregger have computed the rate of production of ionization corresponding to this solar flux. We have repeated their calculations for the model atmospheres in Table 1 and a comparison of the noon ionization rates is given in Figure 1. The relative production of O^+ , O_2^+ and N_2^+ ions are of interest and these are shown in Figures 2 and 3. The accuracy of the absorption and photoionization cross sections used is very uncertain and Figures 1 and 2 should be regarded as merely representative of the actual ionization rates.

Table 1
Atmospheric Temperatures and Number Densities

Altitude (Km)	T _g (°K)	T(∞) = 1,000°K			T(∞) = 2,000°K				
		n(0)	n(O ₂)	n(N ₂)	n _e	T _g (°K)	n(0)	n(O ₂)	n(N ₂)
500	1,000	1.03(7)	2.14(4)	6.36(5)	1.05(6)	2,000	7.14(7)	2.02(6)	3.12(7)
450	1,000	2.36(7)	1.11(5)	2.69(6)	1.24(6)	1,970	1.09(8)	4.69(6)	6.53(7)
400	1,000	5.44(7)	5.92(5)	1.16(7)	1.44(6)	1,940	1.70(8)	1.12(7)	1.40(8)
350	1,000	1.27(8)	3.24(6)	5.14(7)	1.63(6)	1,895	2.70(8)	2.77(7)	3.10(8)
300	998	3.02(8)	1.82(7)	2.33(8)	1.66(6)	1,810	4.49(8)	7.31(7)	7.30(8)
250	990	7.32(8)	1.06(8)	1.09(9)	1.17(6)	1,660	8.07(8)	2.17(8)	1.91(9)
200	952	1.89(9)	6.83(8)	5.59(9)	7.20(5)	1,390	1.72(9)	8.25(8)	6.29(9)
150	763	6.59(9)	6.63(9)	4.20(10)	4.60(5)	880	5.99(9)	6.33(9)	3.96(10)
120	380	3.40(10)	8.80(10)	4.40(11)	3.20(5)	380	3.40(10)	8.80(10)	4.40(11)

+ 1.03(7) = 1.03 × 10⁷ cm⁻³

Table 2

Solar Spectral Intensities at Normal Incidence

λ (in Å)	Flux (in $10^8 \text{ cm}^{-2} \text{ sec}^{-1}$)	λ (in Å)	Flux (in $10^8 \text{ cm}^{-2} \text{ sec}^{-1}$)
1025.7	26	500 - 600	30
1000 - 1027	15	400 - 500	24
989.8	5	303.8	43
977.0	30	300 - 400	29
972.5	10	230 - 300	31
949.7	5	170 - 230	33
911 - 1000	37	110 - 170	3.5
850 - 911	95	80 - 110	2.4
796 - 850	25	60 - 80	1.8
700 - 796	50	30 - 60	1.5
600 - 700	47	20 - 30	0.12
584.3	29	10 - 20	0.02

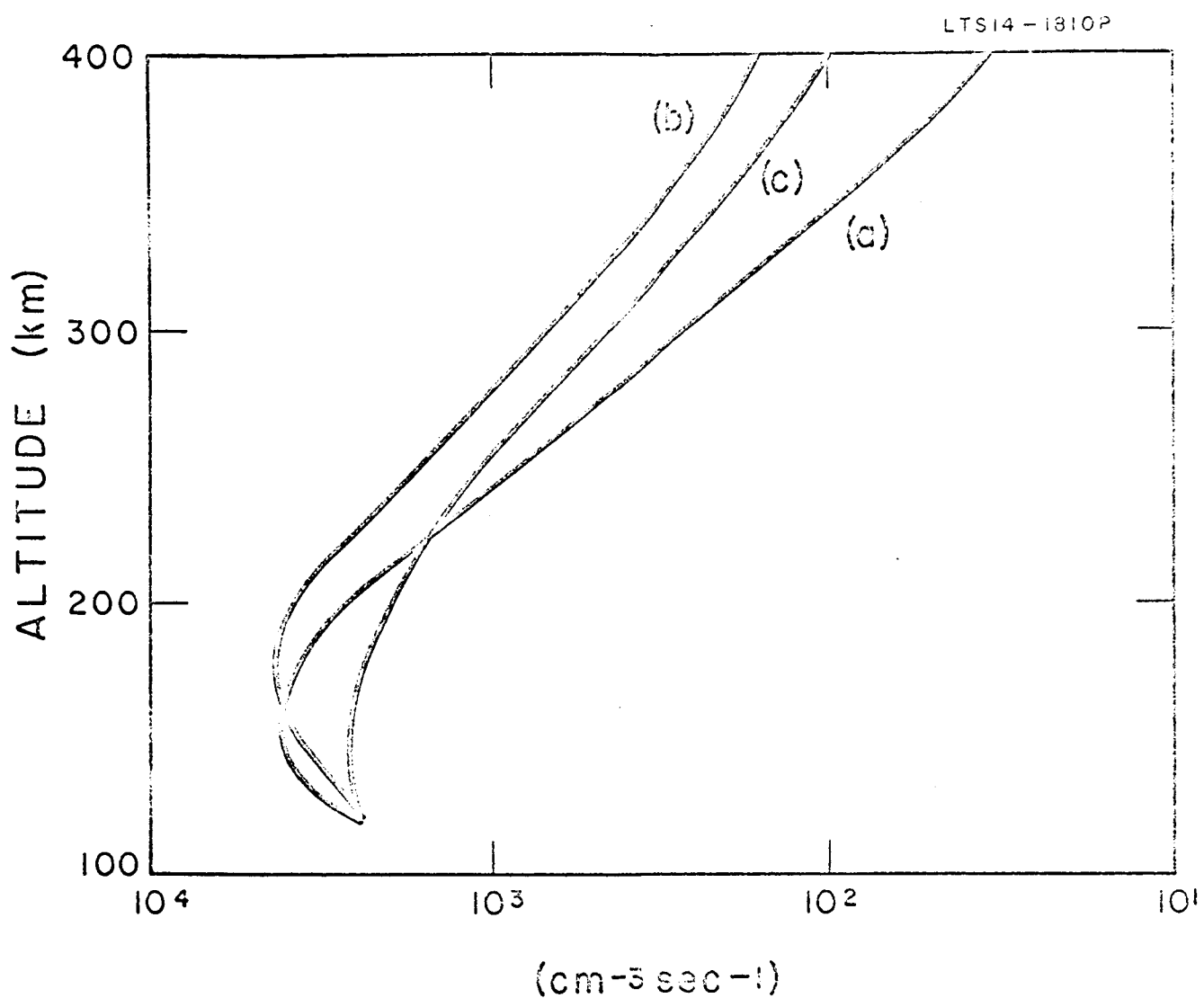


Figure 1. Noon total photoionization rates:
Curve (a) $T(\infty) = 1000^\circ\text{K}$
(b) $T(\infty) = 2000^\circ\text{K}$
(c) Watanabe and Hinteregger (1962)

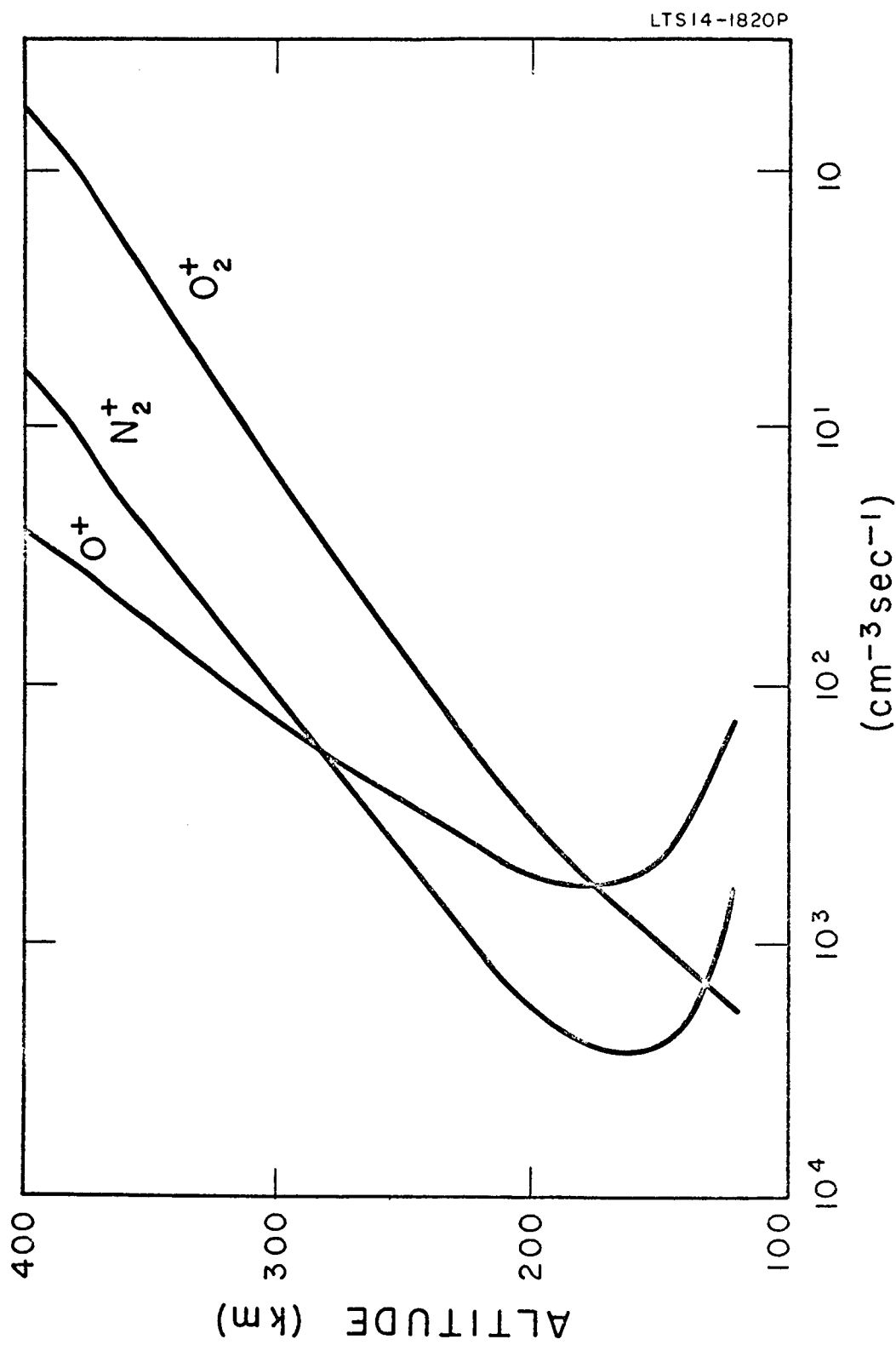


Figure 2. Noon photoionization rates for $T(\infty) = 1000\text{K}$ for O^+ , O_2^+ and N_2^+ .

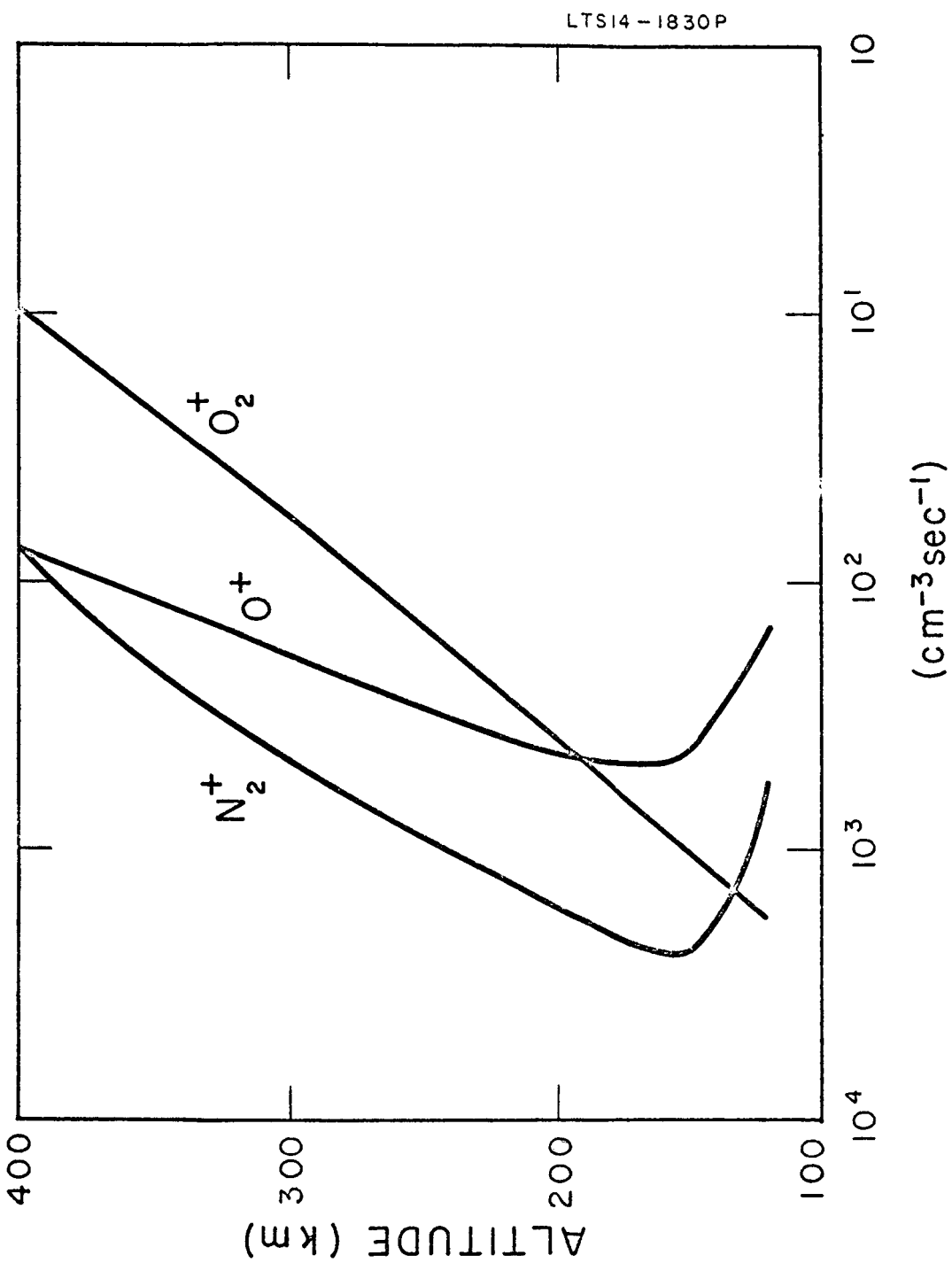


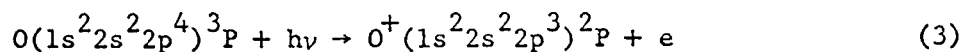
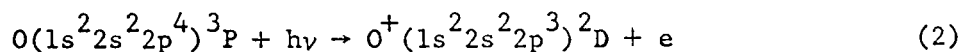
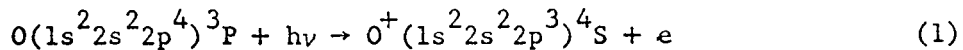
Figure 3. Noon photoionization rates for $T(\infty) = 2000^\circ\text{K}$ for O_2^+ , O^+ and N_2^+ .

2.3 Equilibrium Electron Densities

Since the rates of the processes responsible for the disappearance of free electrons are still very uncertain, we have not attempted to calculate the equilibrium distributions of the electron density as functions of altitude for the assumed models but we have instead adopted the values given by Ratcliffe (1960) and listed in Table 1.

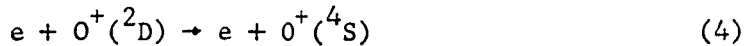
2.4 Energy Distribution of Photoelectrons

The prediction of the energy distribution of the photoelectrons is complicated by the fact that the available cross section data refer to a multiplicity of ionizing processes whereas the energy distribution depends upon the individual processes. Thus, the spectral heads for the ejection of an outer shell electron from atomic oxygen for the transitions

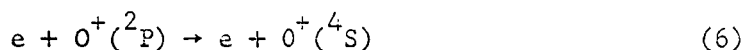
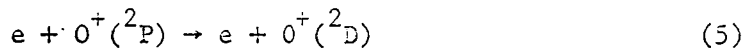


are located at 910\AA , 732\AA and 663\AA , respectively, so that a photon of wavelength, say 500\AA , absorbed by atomic oxygen will produce an electron of energy 11.2eV, 7.9eV or 6.1eV depending upon which transition is involved. The internal energies of the metastable ions may still be

available as heating. Thus, the radiative lifetime of the $^2D_{3/2}$ state is 5×10^3 sec and of the $^2D_{5/2}$ state is 2×10^4 sec; and the rate coefficient for the superelastic collision



is about $3 \times 10^{-8} \text{ cm}^3 \text{ sec}^{-1}$ (Seaton and Osterbrock 1957). The metastable energy of the 2D state may therefore be transferred directly to the ambient electron gas. Alternatively, the metastable ion may undergo ion-atom interchange with the atmospheric molecules, its energy thereby appearing as thermal energy of the heavy particle gas. The radiative lifetime of the $^2P_{1/2}$ state is 5 sec and of the $^2P_{3/2}$ state is 4 sec and the rate coefficients for the superelastic collisions

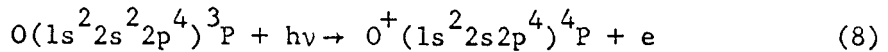


are, respectively, about $1 \times 10^{-7} \text{ cm}^3 \text{ sec}^{-1}$ and $2 \times 10^{-8} \text{ cm}^3 \text{ sec}^{-1}$ (Seaton and Osterbrock 1957). Except at low altitudes where ion-atom interchange may occur more rapidly, the 2P state is usually deactivated by spontaneous emission, the more probable process being

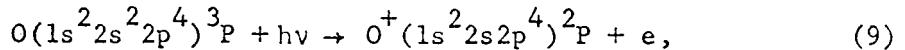


yielding a photon of wavelength 7330 Å and leaving a metastable 2D state, the energy of which may be transferred to the ambient electrons or to the heavy particles.

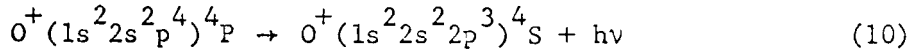
At 435 Å, the photoionizing transition



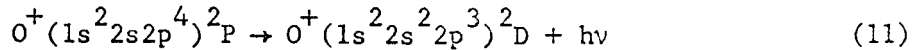
and at 310 Å, the photoionizing transition



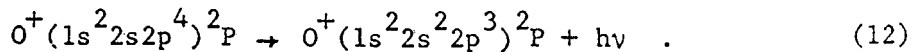
which involve the ejection of an inner shell electron, can occur (Dalgarno and Parkinson 1960). The excited state produced by (8) will subsequently decay according to



with the emission of a photon of wavelength 833 Å which can be absorbed by atomic oxygen yielding an electron with an energy of 1.2 eV or by molecular oxygen yielding an electron of energy 2.7 eV. The excited state produced by (9) will decay according to



or according to



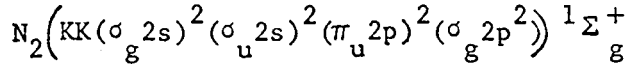
The photons emitted in (11) and (12) have wavelengths of 581 Å and 537 Å, respectively, and can produce further ionization. As before, the metastable states in (11) and (12) may be deactivated by super-elastic collisions.

Radiation of wavelengths between 310 Å and the K-shell absorption edge at about 23 Å can produce electrons with energies ranging from zero to 540 eV. These high energy electrons will in turn produce further electrons by impact ionization. For initial energies greater than perhaps 70 eV the mean number of ion pairs produced can be obtained by dividing the initial energy by 34 eV but below 70 eV the mean energy required to produce an ion pair must rise rapidly as an increasing fraction of the energy is expended in excitation processes (cf. Dalgarno and Griffing 1958). In computing the ionization rates of Figure 1, we have arbitrarily assumed that for electron energies between 20 and 70 eV, one ion pair is produced.

We shall not discuss the absorption of radiation shorter than 23 Å in detail. For our purposes it suffices to note that the solar flux of photons with wavelengths shorter than 30 Å is of the order of $0.1 \text{ erg cm}^{-2} \text{ sec}^{-1}$ and that it is largely deposited in the E-region of the ionosphere.

The photoionization pattern for the atmospheric molecules is basically similar to but, because of the vibrational structure, more complex than that of atomic oxygen.

The first ionization potential of molecular nitrogen is equivalent in energy to a wavelength of 796 Å and corresponds to the removal of a σ_g 2p electron from the N₂ ground state configuration

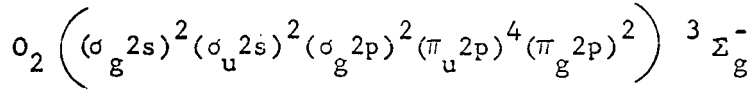


leaving an N₂⁺ molecule in its ground electronic $^2\Sigma_g^+$ state. At a slightly shorter wavelength, a π_u 2p electron can be ejected, yielding N₂⁺ in an excited $^2\pi_u$ state, and at 661 Å, an inner shell σ_u (2s) can be ejected, yielding N₂⁺ in an excited $^2\Sigma_u^+$ state. Presumably both the $^2\pi_u$ and $^2\Sigma_u^+$ states are deactivated by spontaneous emission, the $^2\Sigma_u^+$ giving rise to the first negative band system. There will be further discontinuities in the photoionization cross sections

associated with the removal of a σ_g (2s) electron and yielding N₂⁺ in an excited $^2\Sigma_g^+$ state. None of these excited states is metastable and there seems to be no possibility of a direct transfer of their energy to the ambient electrons. They are of interest, however, within the context of the heat balance of the high atmosphere for they provide a mechanism by which some of the incident solar energy is converted directly into radiation and so rendered unavailable for heating.

The first ionization potential of molecular oxygen is equivalent in energy to a wavelength of 1016 Å and corresponds to the removal of

a π_g 2p electron from the O_2 ground state configuration



leaving an O_2^+ molecule in its ground electronic $^2\pi_g$ state. At a wavelength of perhaps 767 Å, a π_u 2p electron can be ejected, yielding an O_2^+ molecule in the excited $^4\pi_u$ state, and at a wavelength of 729 Å, it can yield an O_2^+ molecule in the excited $^2\pi_u$ state. The σ_g 2p electron can be ejected at a wavelength of perhaps 681 Å, yielding O_2^+ in the $^4\Sigma_g^-$ state and there will be other discontinuities at shorter wavelengths associated with the removal of σ_u 2s and σ_g 2s electrons, yielding further O_2^+ in $^2\pi_u$ and $^2\pi_g$ states. The $^2\pi_u$ and $^4\Sigma_g^-$ states are the upper states of the first and second negative band systems, the latter of which terminates in the $^4\pi_u$ state. The $^4\pi_u$ state is metastable and its energy of about 4eV may be transferred directly to the ambient electron gas by superelastic collisions.

The transformation of this essentially qualitative discussion into a quantitative prediction of the energy distribution of the photoelectrons must be somewhat arbitrary. For the photoionization cross sections, we have used the values listed by Watanabe and Hinteregger (1962) and we have assumed that whenever the photon energy is such that a multiplicity of transitions can occur the probability of a particular transition is proportional to the statistical weight of the product positive ion state. The transitions

which have been taken into account are given in Table 3.

The resulting distributions with altitude of the rates of production of photoelectrons of various energies arising from the transition (1) are illustrated in Figures 4 and 5 for the two model atmospheres. Similar curves may be constructed for the other photoionizing processes. The total rates of deposition of photo-electron kinetic energy are given in Figures 6 and 7 which also show the distributions with altitude of the rates of deposition of energy retained initially in the metastable states $O^+(^2D)$ and $O_2^+(^4\pi_u)$. Part of the energy will subsequently be converted into radiation and the remainder into heat, the division depending upon the collision processes by which the fast electrons are slowed down.

Table 3
 Transitions Taken Into Account in Deriving the Energy
 Distribution of Photoelectrons

Atomic Oxygen Transitions

<u>Electron removed</u>	<u>Resulting state of O⁺</u>	<u>Threshold energy in eV</u>
2p	⁴ S	13.6
2p	² D	16.9
2p	² P	18.7
2s	⁴ P	28.5
2s	² P	40.0

Molecular Oxygen Transitions

<u>Electron removed</u>	<u>Resulting state of O₂⁺</u>	<u>Threshold energy in eV</u>
π_g 2p	² π_g	12.1
π_u 2p	⁴ π_u	16.2
π_u 2p	² π_u	17.0
σ_g 2p	⁴ Σ_g^-	18.2
σ_u 2s	² π_u	\sim 28
σ_g 2s	² π_g	\sim 40

Molecular nitrogen transitions

<u>Electron removed</u>	<u>Resulting state of N₂⁺</u>	<u>Threshold energy in eV</u>
σ_g 2p	² Σ_g^+	15.6
π_u 2p	² π_u	16.7
σ_u 2s	² Σ_u^+	18.8
σ_g 2s	² Σ_g^+	\sim 35

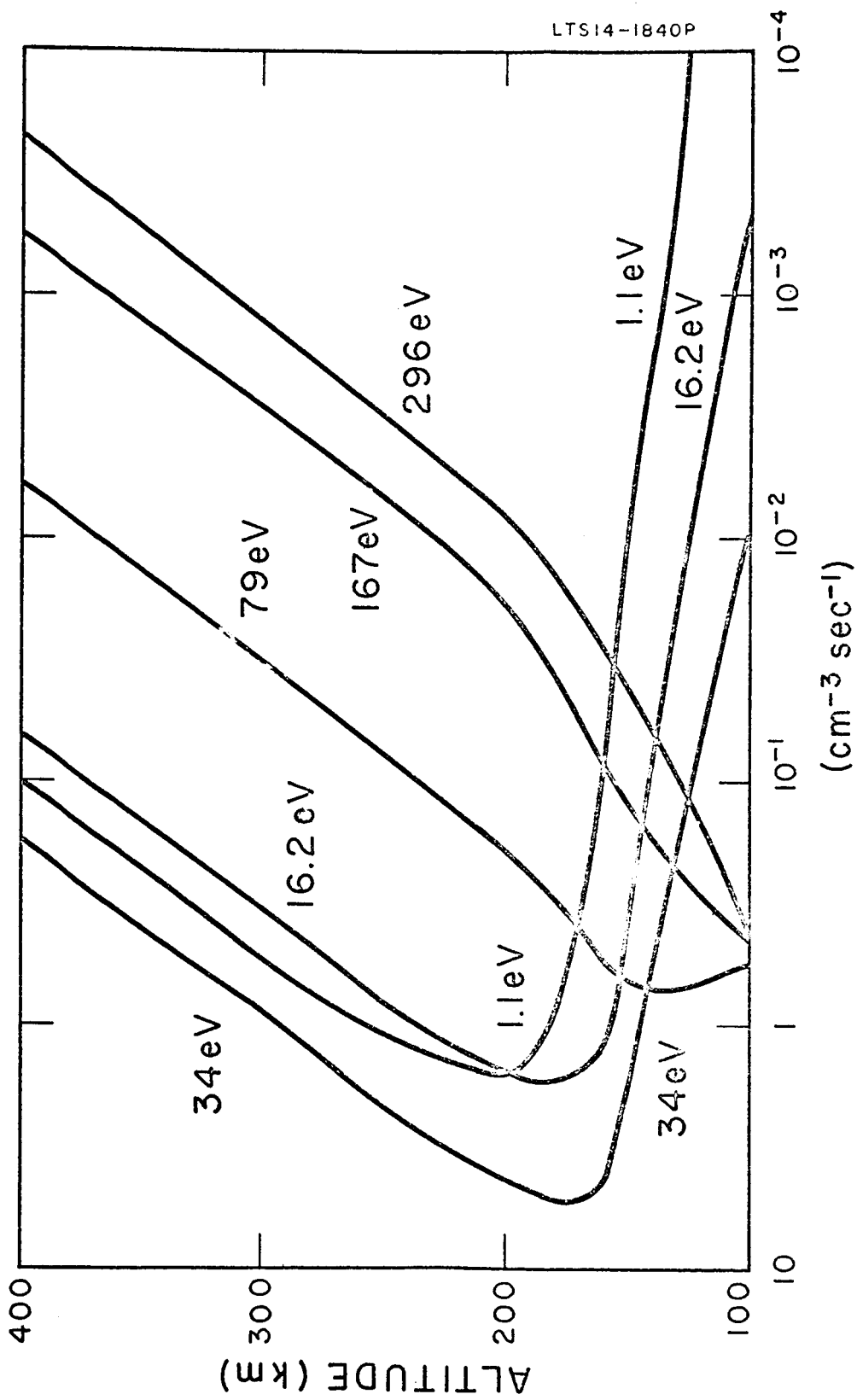


Figure 4. Distribution of photoelectrons produced by process (1)
for $T(\infty) = 1000^\circ\text{K}$.

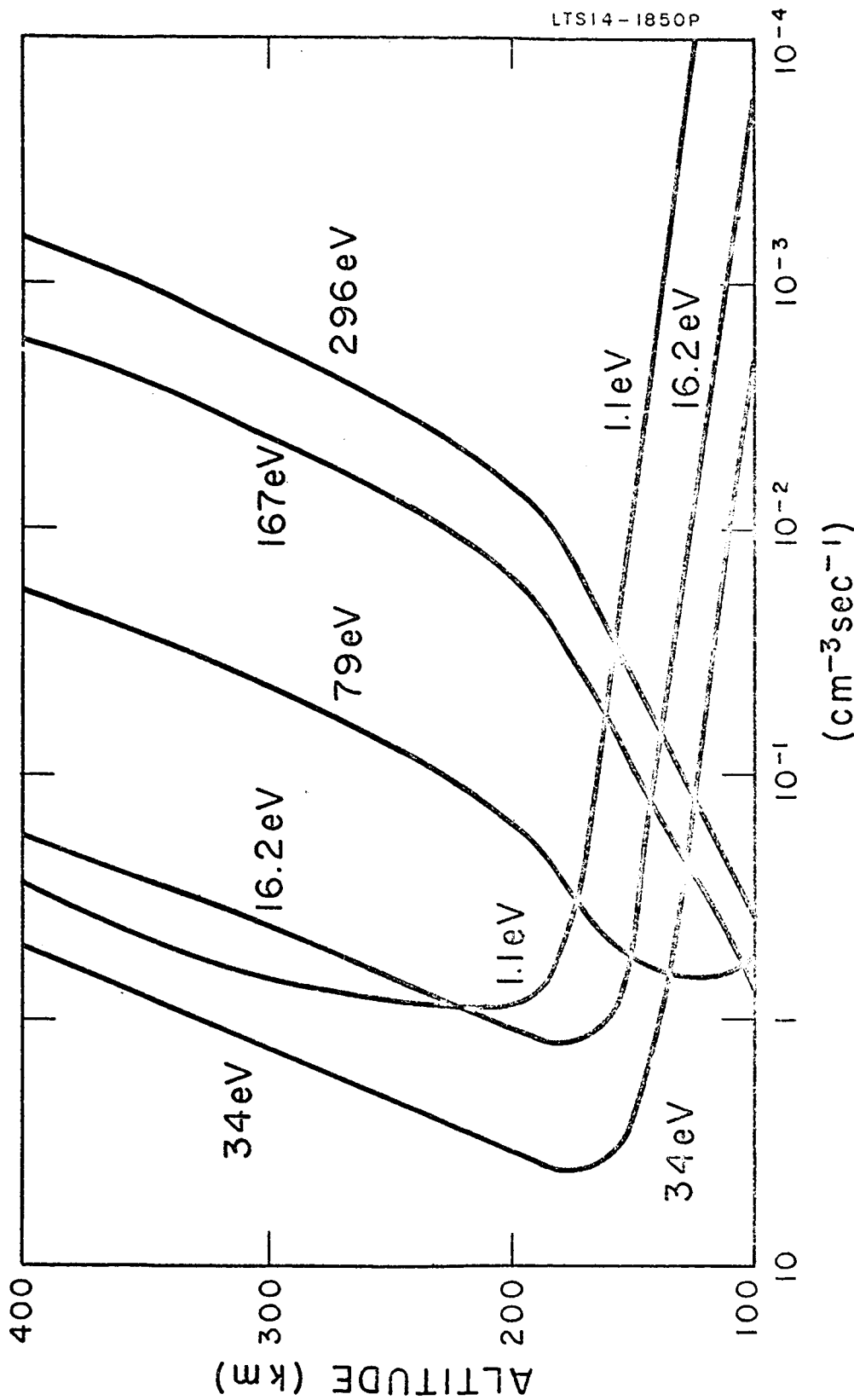


Figure 5. Distribution of photoelectron sproduced by process (1)
for $T(\infty) = 2000^\circ\text{K}$.

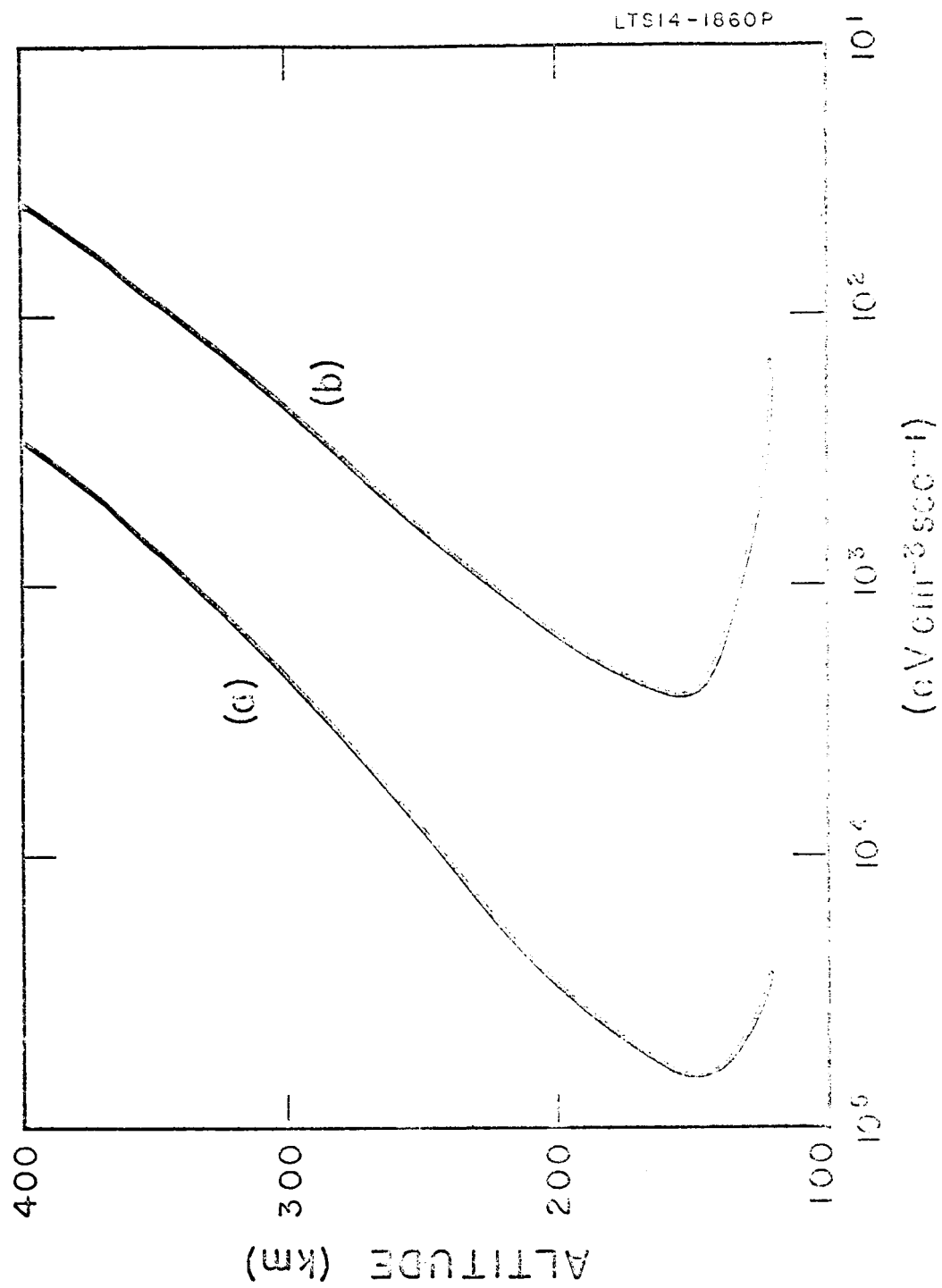


Figure 6. Total rate of deposition of photoelectron kinetic energy (curve a) and of metastable energy (curve b) for $T(\infty) = 1000^\circ\text{K}$.

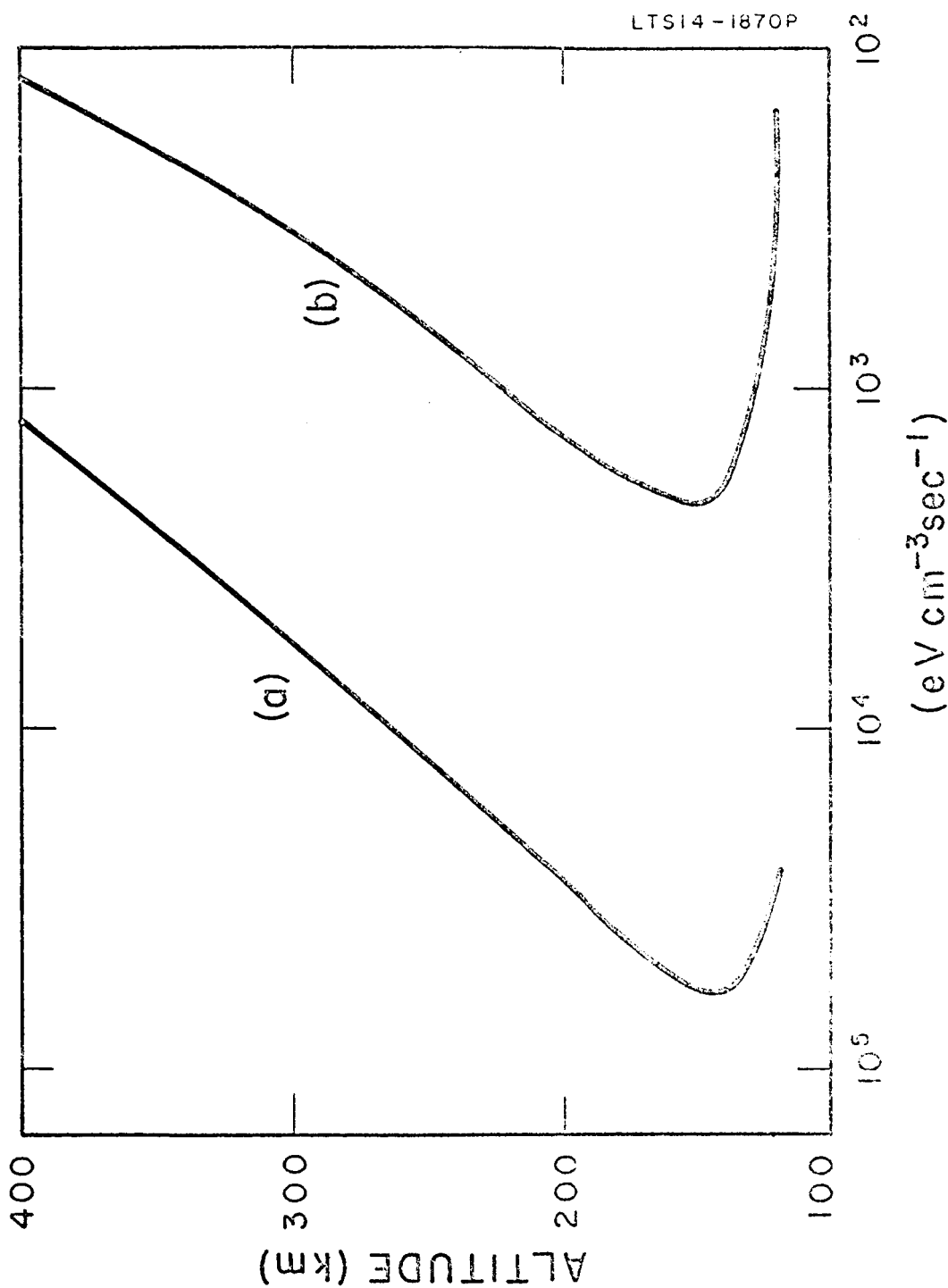


Figure 7. Total rate of deposition of photoelectron kinetic energy (curve a) and of metastable energy (curve b) for $T(\infty) = 2000^\circ\text{K}$.

3. Energy Loss Processes

3.1 Excitation and Ionization

The rate of energy loss per cm of path by optically allowed excitation and ionization processes for a high energy electron moving through air with a number density $n \text{ cm}^{-3}$ is given by the Bethe formula (ignoring relativistic effects)

$$\frac{dE}{dx} = - n \frac{1.87 \times 10^{-12}}{E} \ln(E/80) \text{ eV cm}^{-1} \quad (13)$$

where E is the energy in eV (cf. Dalgarno 1961). The Bethe formula (13) remains valid to well within an order of magnitude down to energies of five hundred electron volts. To obtain the energy loss rate at lower energies we assume that for incident energies greater than 50 eV, the efficiencies of ionization processes and excitation processes are equal and that the mean energy loss for each ionizing collision is 20 eV. The rate of energy loss can then be obtained using the measured values of the cross sections for the electron impact ionization of the atmospheric gases (Tate and Smith 1932, Fite and Brackman 1959, Rothe, Marino, Neynaber and Trujillo 1962). At 500 eV, this procedure yields an energy loss rate in air of $6 \times 10^{-15} n \text{ eV cm}^{-1}$ in harmony with that derived from (13). For energies between 50 eV and 20 eV we assume that the efficiency of

excitation in slowing down the electron is twice that of ionization and that the mean energy lost in each ionizing process is 15 eV.

These procedures are somewhat arbitrary but are unlikely to lead to errors exceeding a factor of three.

The derived rates of energy loss for electrons with energies ranging from 10 keV to 20 eV are given in Table 4 for air of unit density and the derived rates corresponding to the two model atmospheres are shown in Figures 8 and 9.

3.2 Excitation to Metastable States

At energies of about 20 eV, energy loss through excitation of the metastable levels of atomic and molecular oxygen and of molecular nitrogen are comparable to the energy loss through allowed transitions, becoming of increasing importance as the energy decreases. Many processes contribute to the energy loss and very few of the relevant cross section data are available. A rough analysis suggests that the mean rate of energy loss in the atmosphere decreases slowly to a value of the order of $10^{-16} n \text{ eV cm}^{-1}$ at an energy of about 7 eV. Below this energy no significant loss is to be expected from excitation of electronic levels of N_2 and the rate of energy loss at altitudes below 300 km will decrease sharply as the energy falls below about 7 eV.

It follows from the cross section calculations of Seaton (1956) that between 7 eV and 3 eV excitations to the metastable 1D and 1S states of atomic oxygen contribute about $5 \times 10^{-17} n (0) \text{ eV cm}^{-1}$ to the

Table 4

Rates of Energy Loss for Electrons in Air of Unit Density

Energy (in eV)	10,000	5,000	1,000	750	500	400	300	200	100	75	50	40	30	20
$-\frac{dE}{dx} \times 10^{15}$ (eV cm ⁻¹)	0.9	1.6	4.7	5.6	6.3	6.8	7.9	9.4	10.8	10.2	8.8	7.0	4.1	1.3

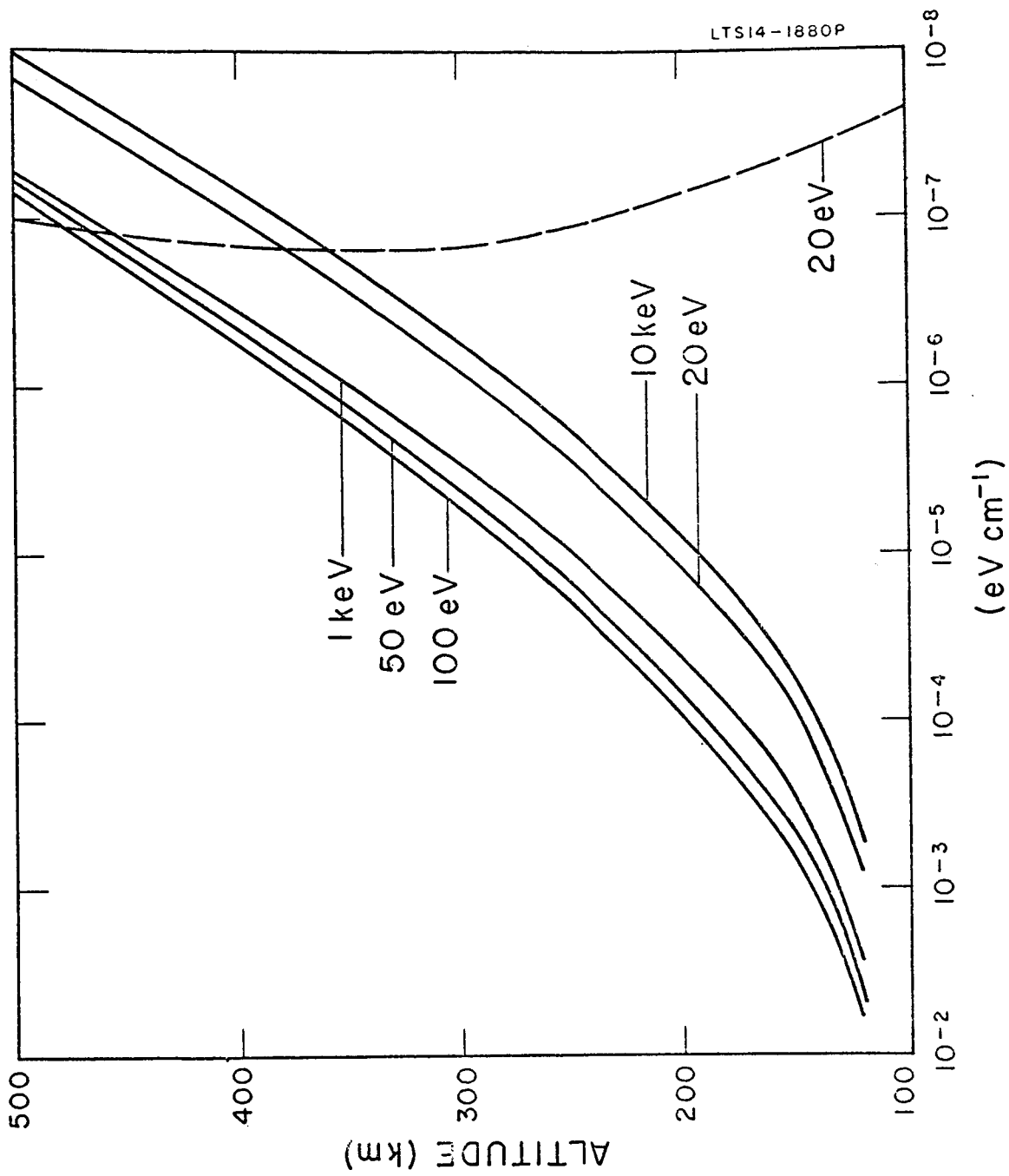


Figure 8. Rates of energy loss to neutral particles (solid lines) and to electrons (dashed line) for electrons of various energies above 20 eV moving in the model atmosphere with $T(\infty) = 1000^{\circ}\text{K}$.

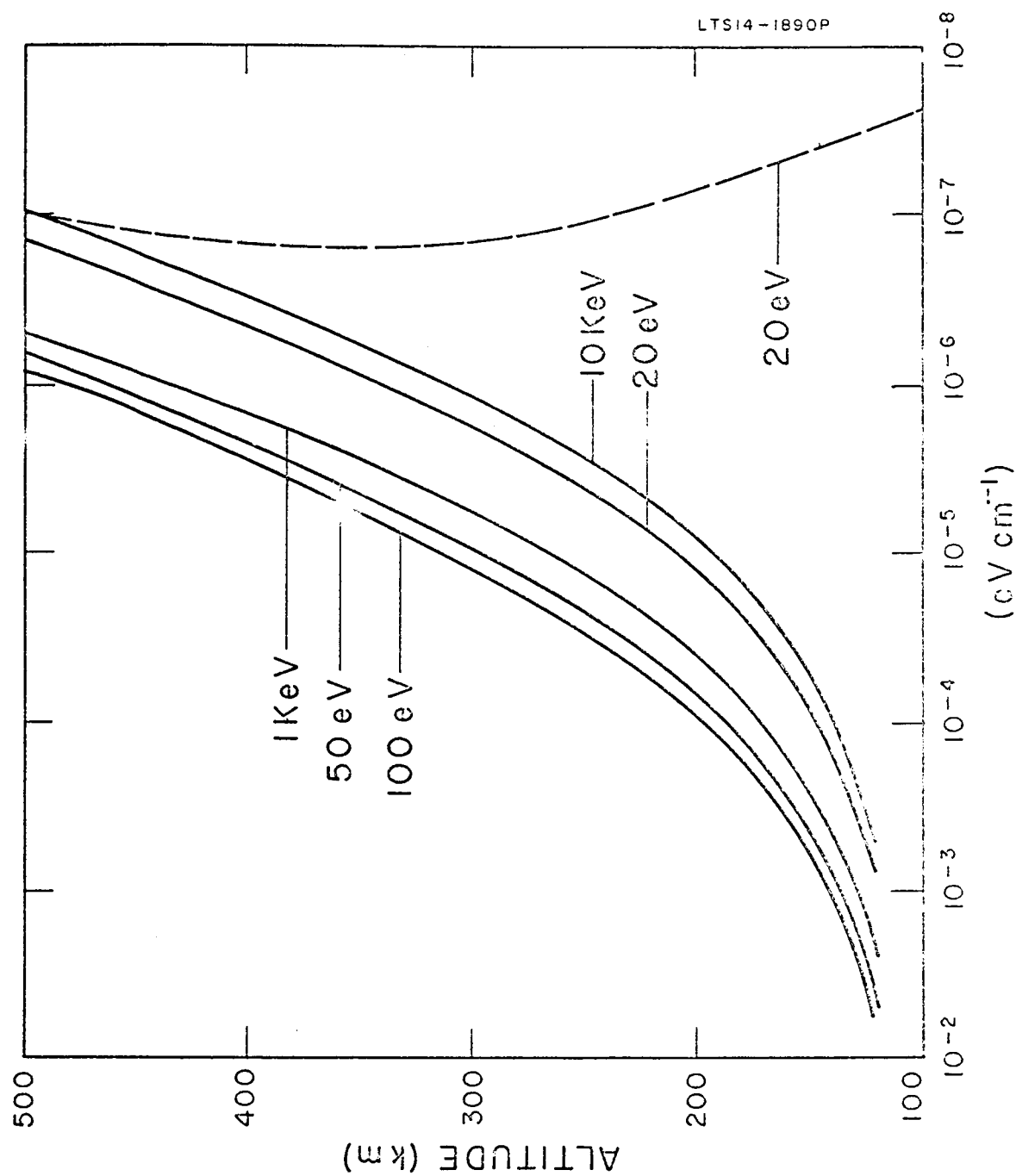


Figure 9. Rates of energy loss to neutral particles (solid lines) and to electrons (dashed line) for electrons of various energies above 20 eV moving in the model atmosphere with $T(\infty) = 20000K$.

rate of energy loss. The contributions of dissociative attachment of molecular oxygen (cf. Thompson 1959) and of excitation to excited electronic levels of molecular oxygen (Schulz and Dowell 1962) are small in comparison and can be ignored at altitudes above 120 km.

The derived rates of energy loss for electrons with energies between 20 eV and 5 eV for the two model atmospheres are shown in Figures 10 and 11.

3.3 Vibrational Excitation of N₂

At energies below about 3.5 eV, energy loss through excitation of the vibrational levels of molecular nitrogen becomes very important. The total cross sections have been measured by Haas (1957) and the relative cross sections for excitation to the individual vibrational levels with quantum number v between 2 and 8 by Schulz (1962). The corresponding rate of energy loss for unit number density of nitrogen is illustrated in Figure 12. It includes an arbitrary estimate of the contribution from excitation to the v = 1 level, the cross section for which has not been measured.

The rates of energy loss appropriate to the two model atmospheres are given in Figures 13 and 14 which include also the contribution of excitation to the metastable levels of atomic oxygen.

The fate of the energy stored as vibrational excitation is uncertain. It may be transferred to the ambient electron gas by

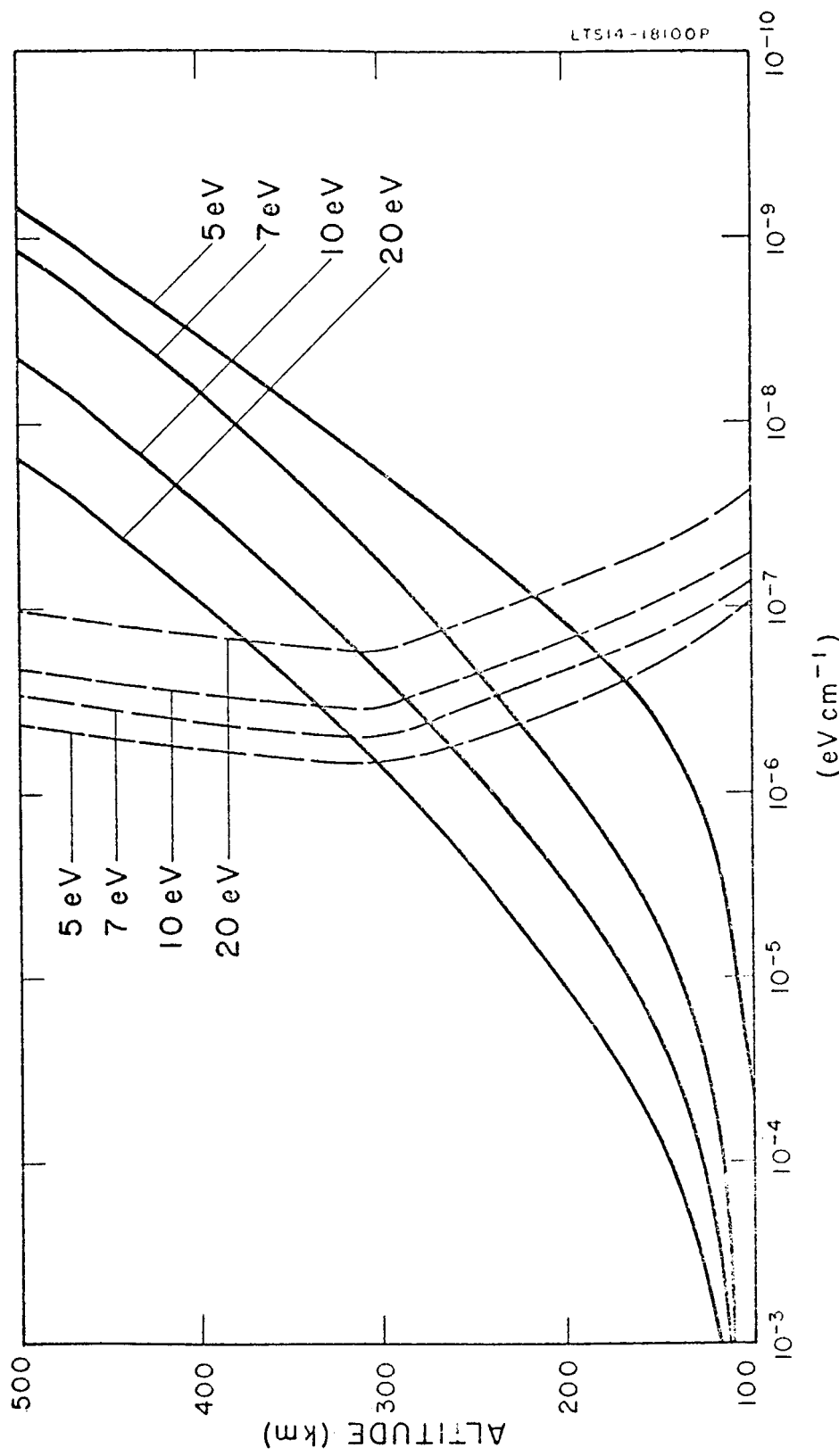


Figure 10. Rates of energy loss to neutral particles (solid lines) and to electrons (dashed lines) for electrons of various energies below 20 eV moving in the model atmosphere with $T(\infty) = 1000^\circ\text{K}$

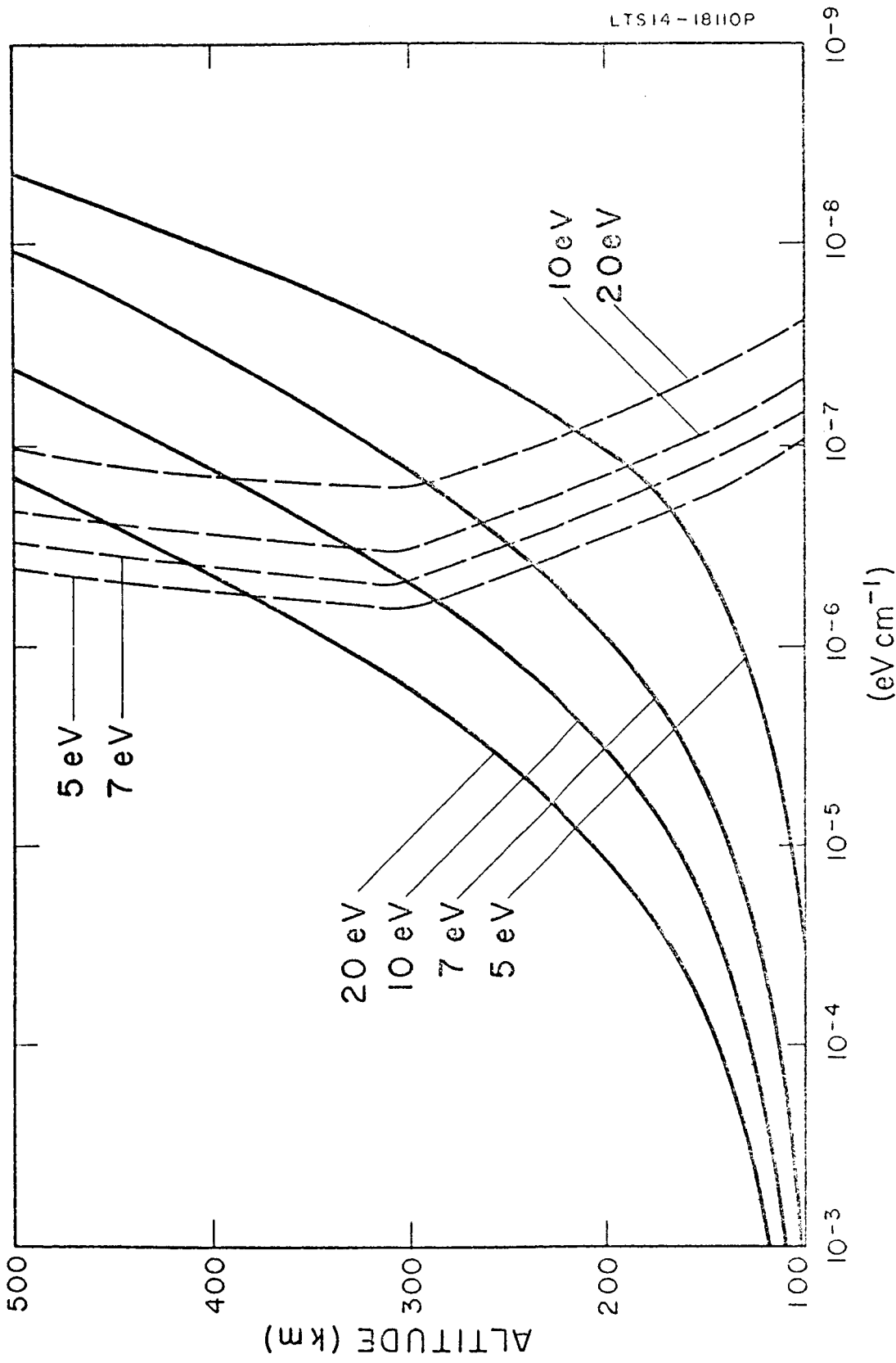


Figure 11. Rates of energy loss to neutral particles (solid lines) and to electrons (dashed lines) for electrons of various energies below 20 eV moving in the model atmosphere with $T(\infty) = 2000^\circ\text{K}$.

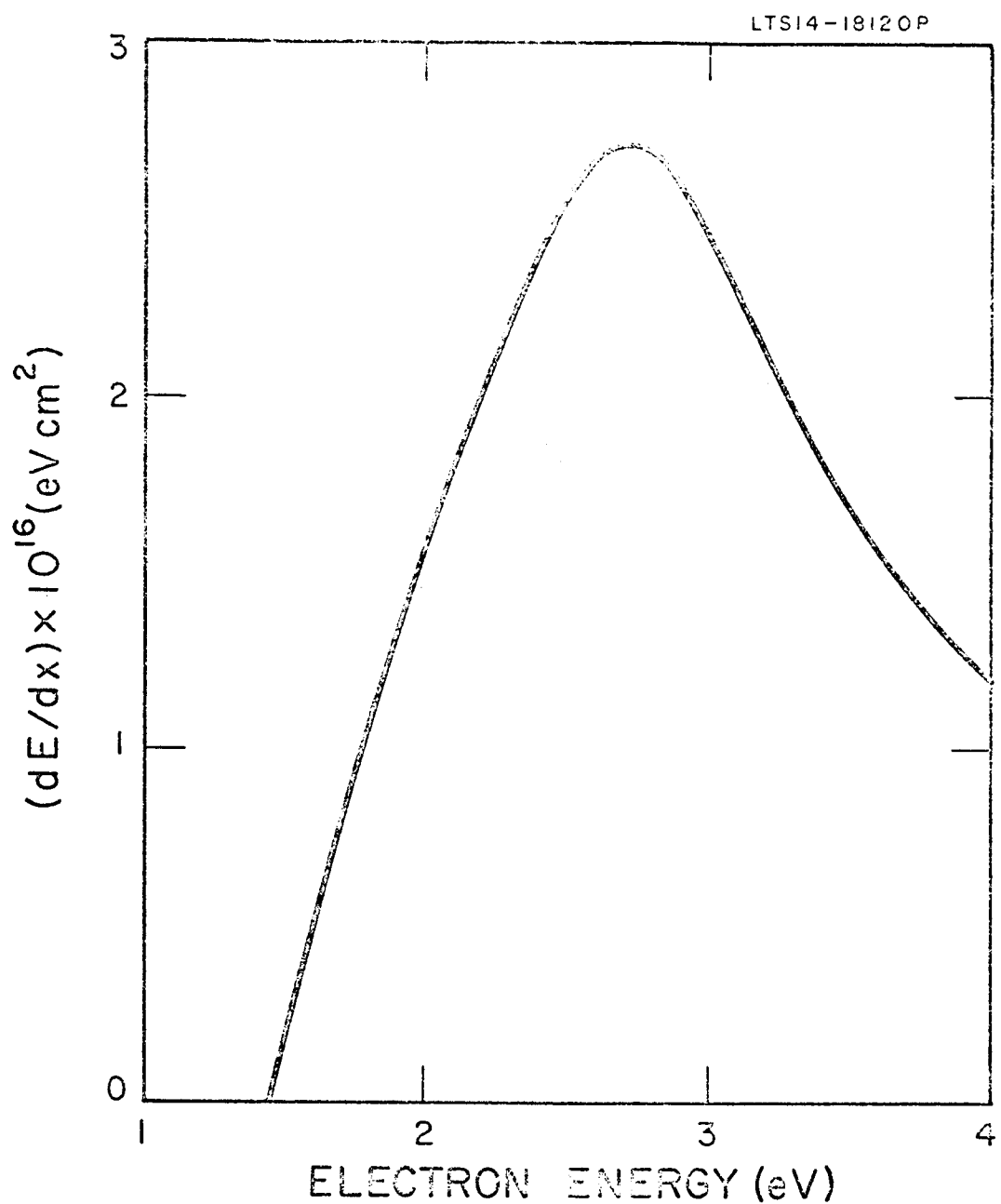


Figure 12. Rates of energy loss through vibrational excitation of molecular nitrogen at unit density.

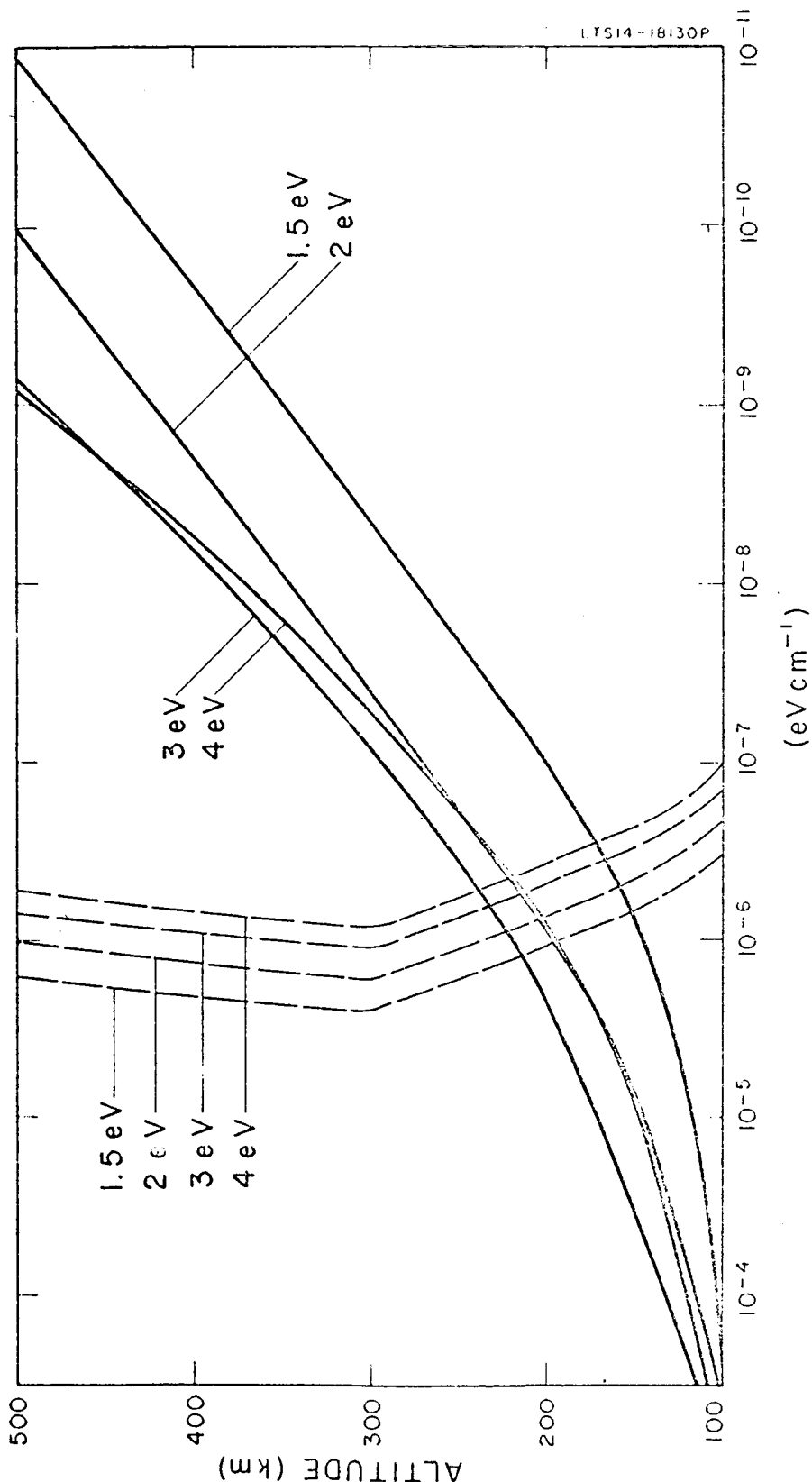


Figure 13. Rates of energy loss to neutral particles (solid lines) and to electrons (dashed lines) for electrons with energies between 1.5 eV and 4 eV moving in the model atmosphere with $T(\infty) = 10000\text{K}$.

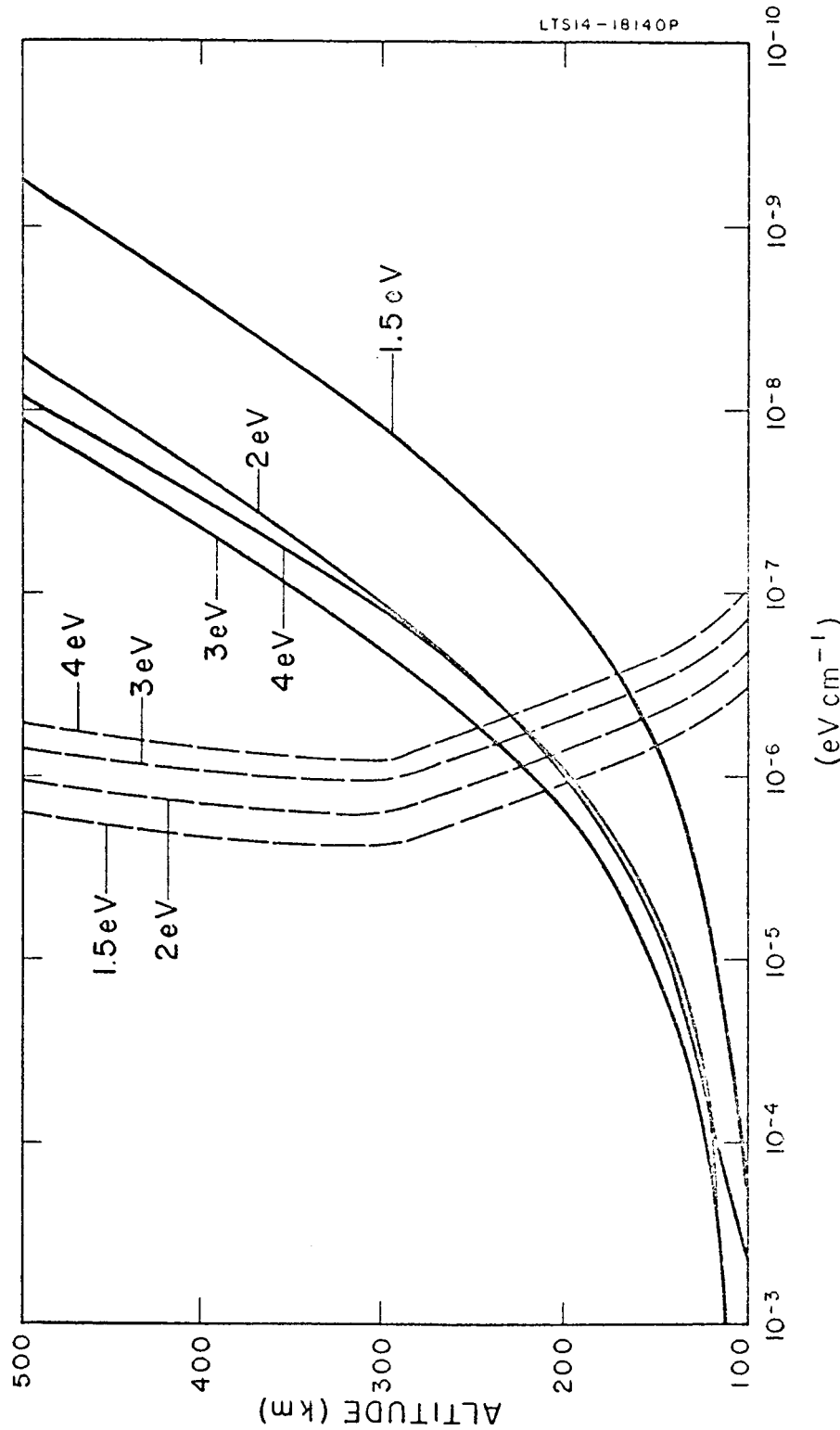
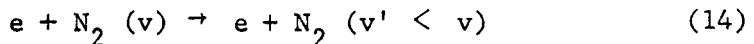


Figure 14. Rates of energy loss to neutral particles and to electrons for electrons with energies between 1.5 eV and 4 eV moving in the model atmosphere with $T(\infty) = 2000^{\circ}\text{K}$.

superelastic collisions



or it may be degraded into kinetic energy of the neutral particles, a possible reaction being atom-atom interchange with atomic nitrogen (Bates 1955, Dalgarno 1963)



The rate coefficient of (14) may be of the order of $10^{-10} \text{ cm}^3 \text{ sec}^{-1}$ but the rate of (15) is unknown except for transitions in which $v' = 0$.

We shall investigate the consequences of both possibilities.

3.4 Rotational Excitation of N_2

Vibrational excitation is rather inefficient at energies below 1.5 eV and the measurements of Schulz and Dowell (1962) suggest that excitation of the $^1\Sigma_g^+$ and $^1\Delta_g$ states of molecular oxygen are very slow processes. As the energy approaches thermal energies, excitation of the rotational levels of N_2 is probably the most efficient loss mechanism, the small quadrupole moment of O_2 causing excitation of the rotational levels of O_2 to be comparatively slow. The rate of energy loss by rotational excitation of N_2 can be obtained from the calculations of Dalgarno and Moffett (1962a) and it is about $5 \times 10^{-20} n(N_2) \text{ eV cm}^2 \text{ sec}^{-1}$. The corresponding rates of energy loss for the two model atmospheres are shown in Figures 15 and 16.

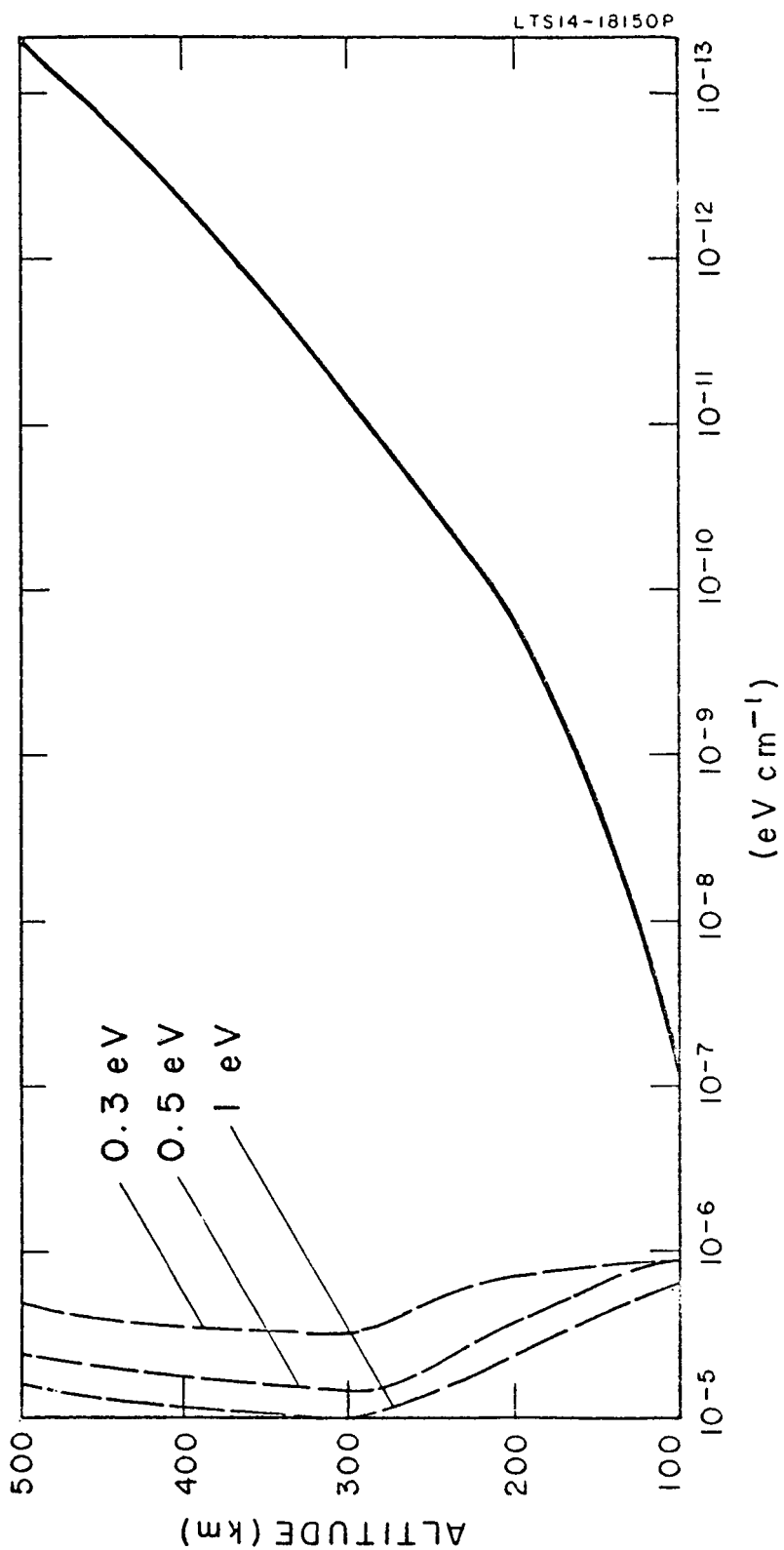


Figure 15. Rates of energy loss through rotational excitation of N_2 (solid lines) and through elastic collisions (dashed lines) with the ambient electrons for $T(\infty) = 1000^\circ\text{K}$.

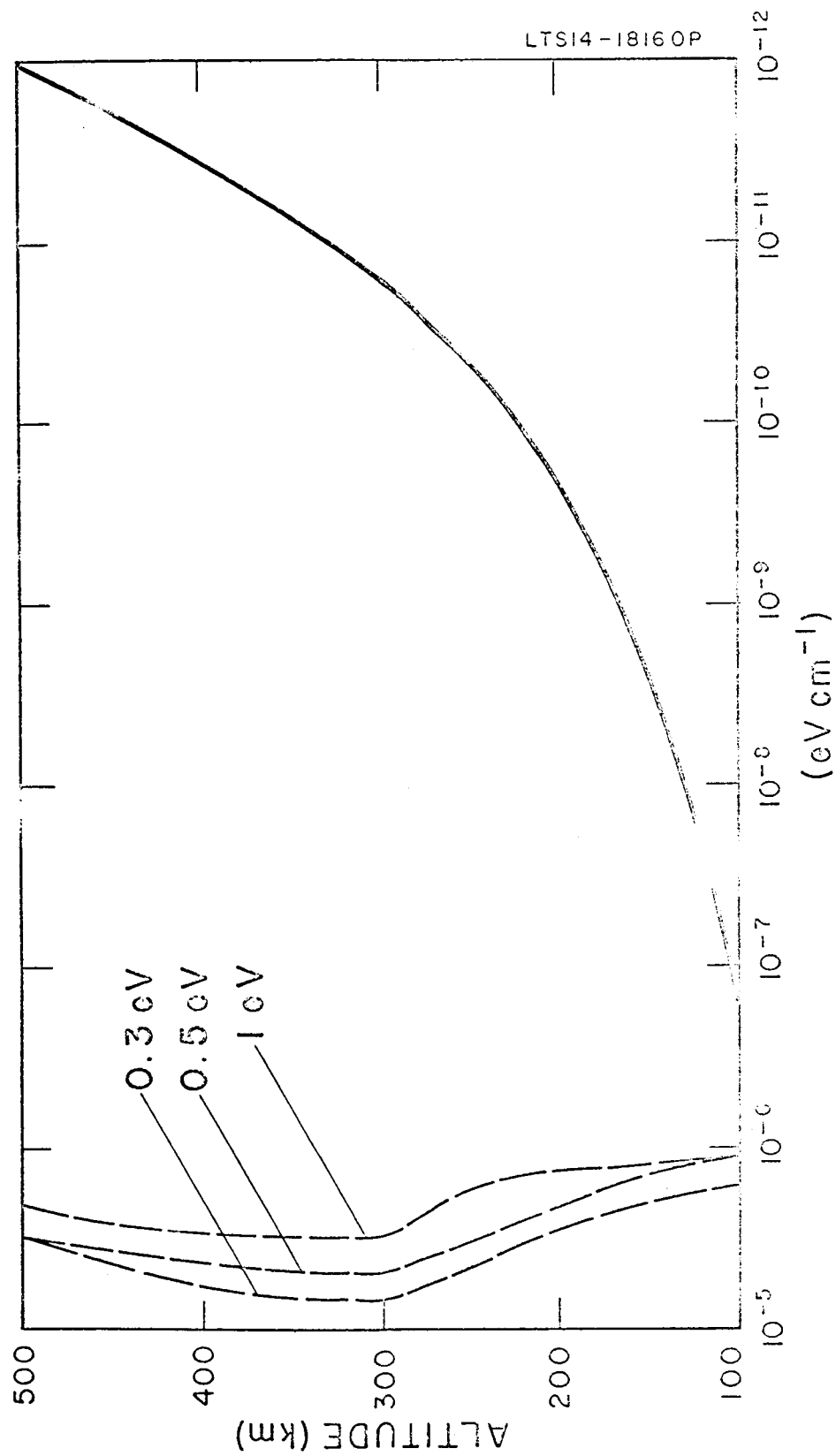


Figure 16. Rates of energy loss through rotational excitation of N_2 (solid lines) and through elastic collisions (dashed lines) with the ambient electrons for $T(\infty) = 2000^\circ\text{K}$.

3.5 Elastic Scattering by Neutral Particles and Positive Ions

The rate of energy loss through elastic scattering by neutral particles is given by

$$-\frac{dE}{dx} = \frac{2m}{M} n EQ_m \quad (16)$$

where m is the mass of the electron, M is the mass of the neutral particle and Q is the cross section for momentum transfer. We shall not present values of (16) since except at energies very close to thermal energies energy loss through rotational excitation is much more efficient. At high altitudes where the concentration of atomic oxygen exceeds that of molecular nitrogen, this is no longer the case but there, loss through elastic scattering by the positive ions is a more efficient mechanism. It is clear, however, from the mass factor in (16) that energy loss through elastic scattering by the positive ions is negligible compared to that through elastic scattering by the ambient electrons.

Although elastic scattering by heavy particles can be ignored in a consideration of the slowing down of the fast photoelectrons, it provides an important mechanism for cooling the heated electron gas and we shall return to it in Section 4.

3.6 Elastic Scattering by Ambient Electrons

In discussing the relative efficiencies of various processes which slow down energetic electrons, we have ignored the elastic

scattering by the ambient electrons, an important process for the selective heating of the ambient electron gas (Hanson and Johnson 1961).

For the mean rate of energy loss through elastic collisions with the ambient electrons, we adopt a formula of Butler and Buckingham (1962)

$$\frac{1}{n_e} \frac{dE}{dx} = - \frac{5.01 \times 10^{-13}}{\sqrt{T_e/1000}} \frac{1}{\sqrt{E}} F \left(\frac{3.41}{\sqrt{T_e/1000}} \right) \ln \lambda \text{ eV cm}^2 \quad (17)$$

where

$$F(x) = \frac{1}{x} \int_0^x \exp(-x^2) dx - 2 \exp(-x^2). \quad (18)$$

The value of $\ln \lambda$ appropriate to the ionospheres of Table 1 is about 15; it is unnecessary for our purposes to take account of its detailed variation with electron temperature and electron density.

Values of (17) are given in Table 5 for a range of incident energies and for several electron temperatures. For energies greater than 3 eV, (17) may be replaced by the asymptotic formula

$$\frac{1}{n_e} \frac{dE}{dx} \sim - \frac{1.95 \times 10^{-12}}{E} \text{ eV cm}^2. \quad (19)$$

The energy loss rates through elastic collisions with the ambient electrons are compared in Figure 8-16 with the energy loss rates corresponding to collisions with the neutral particles.

Table 5
Elastic Loss to Ambient Electrons (in 10^{-12} eV cm 2) +

E (eV) \ T ($^{\circ}$ K)	300	600	900	1200	1500	1800	2100	3000
0.1	17.63	9.74	3.66	- 0.13	- 2.51	- 3.44	- 5.04	- 6.49
0.2	9.74	8.81	6.87	4.87	3.18	1.83	0.77	- 1.25
0.3	6.51	6.40	5.88	5.04	4.01	3.25	2.47	0.73
0.4	4.88	4.87	4.73	4.41	3.95	3.43	2.92	1.59
0.5	3.91	3.90	3.87	3.75	3.53	3.24	2.91	1.95
0.6	3.26	3.25	3.25	3.25	3.10	2.94	2.74	2.06
0.7	2.79	2.79	2.79	2.79	2.72	2.64	2.51	2.05
0.8	2.44	2.44	2.44	2.44	2.41	2.37	2.30	1.97
0.9	2.17	2.17	2.17	2.17	2.16	2.13	2.09	1.87
1.0	1.95	1.95	1.95	1.95	1.95	1.93	1.91	1.76
2.0	0.98	0.98	0.98	0.98	0.98	0.98	0.98	0.97
3.0	0.65	0.65	0.65	0.65	0.65	0.65	0.65	0.65

$\ell_n \lambda$ is taken to be 15.

3.7 Critical Altitudes and Energies

The results of the comparisons of the efficiencies of energy loss to the neutral particles and to the electrons are summarized in Table 6 which gives for various electron energies the critical altitudes for the two model atmospheres above which loss to the electrons is the more probable and below which loss to the neutral particles is the more probable, it being assumed that vibrational energy of N_2 is converted to thermal energy of the neutral particle gas. If we assume that vibrational energy of N_2 is converted to thermal energy of the electron gas, the critical altitudes are unchanged for $E \geq 5$ eV but do not exist for lower energies, all of the electron kinetic energy below 5 eV being transferred to the ambient electrons.

We may summarize the results also by introducing critical energies E_c which are such that for $E > E_c$, E_c is transferred to the electron gas and for $E < E_c$, E is transferred to the electron gas. The critical energies are shown in Figures 17 and 18 for the two model atmospheres corresponding to the alternative assumptions that vibrational energy of N_2 is converted to thermal energy of the neutral particle gas and that it is converted to thermal energy of the electron gas.

Table 6

Critical Altitudes

$T(\infty) = 1,000^{\circ}\text{K}$		$T(\infty) = 2,000^{\circ}\text{K}$	
Energy (eV)	h_c (km)	Energy (eV)	h_c (km)
40	500	18	500
20	370	14	408
10	286	10	332
8	260	8	276
7	236	7	252
6	178	6	176
5	170	5	170
4	220	4	230
3	224	3	240
2	204	2	210
1.5	152	1.5	150

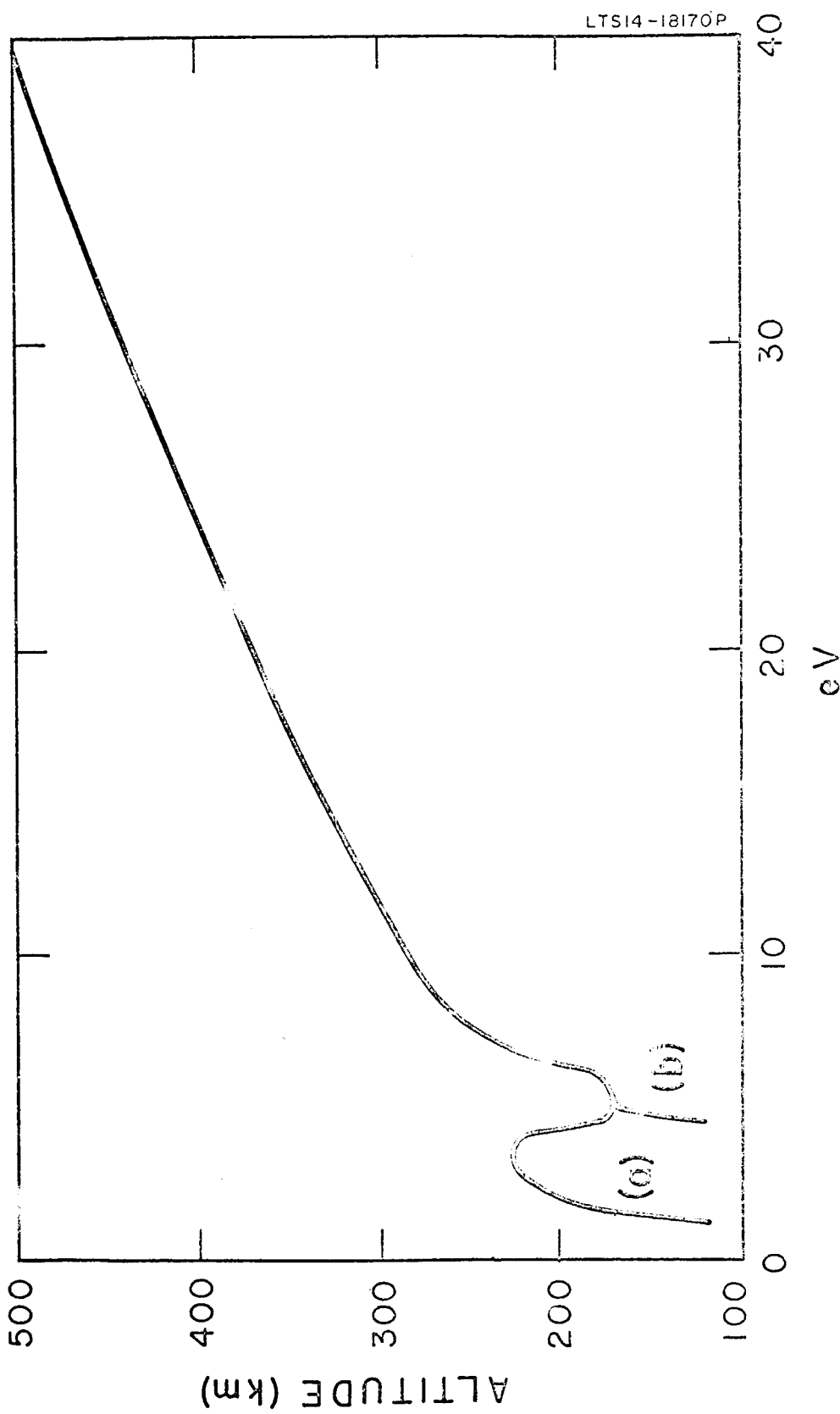


Figure 17. Critical energies for the model atmosphere with $T(\infty) = 1000^{\circ}\text{K}$, assuming that the vibrational energy of N_2 is converted to thermal energy of (a) the neutral particles and (b) the electron gas.

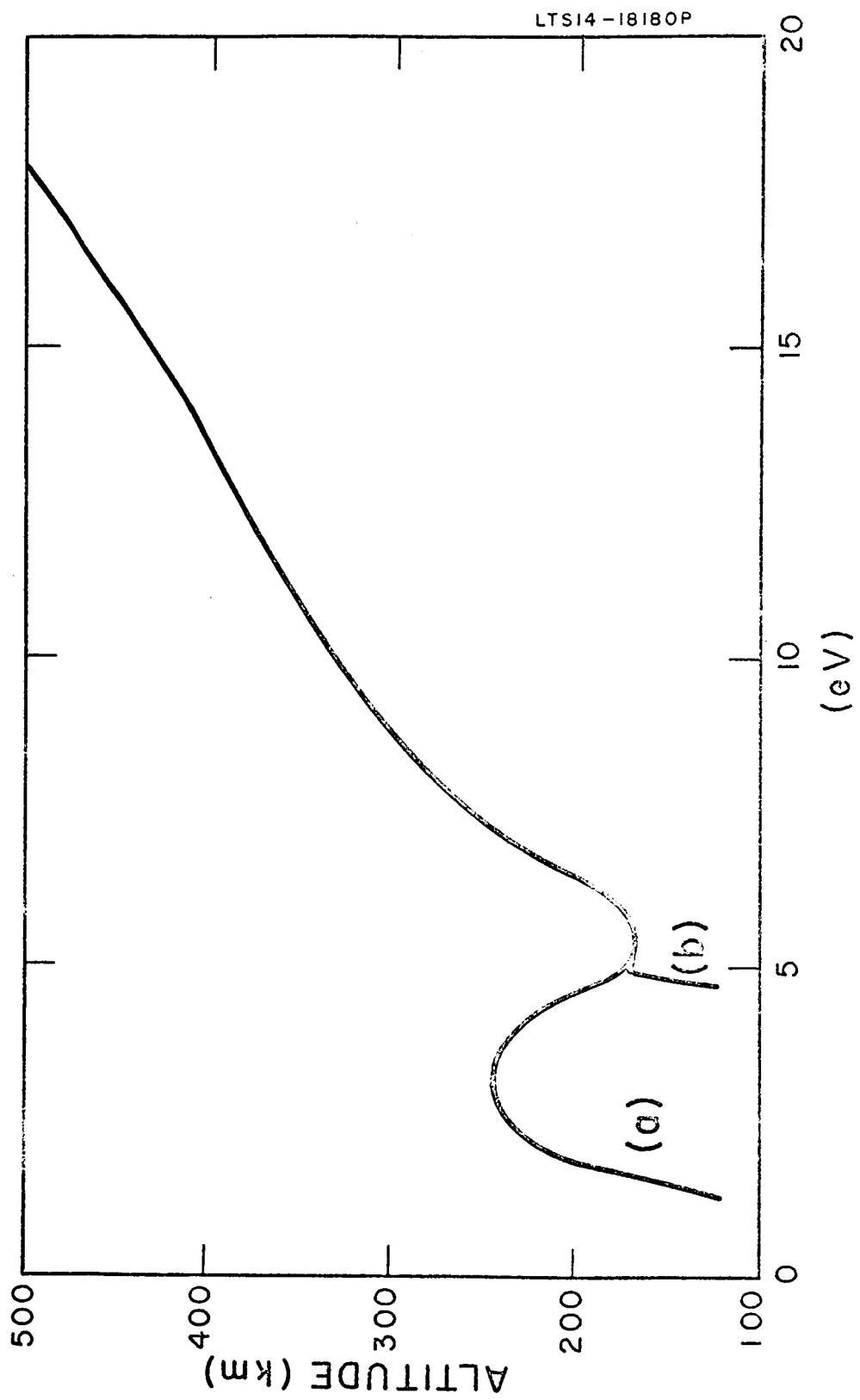


Figure 18. Critical energies for the model atmosphere with $T_{\infty} = 2000^{\circ}\text{K}$, assuming that vibrational energy of N_2 is converted to thermal energy of (a) the neutral particles and (b) the electron gas.

4. Heat Flux and Cooling Processes

Combining the predicted initial energy distribution of the photoelectrons with the critical altitudes and energies yields the distribution of energy which is transferred to the ambient electrons. The results are shown in Figures 19 and 20, there being four distributions for each atmosphere depending upon the ultimate fate of the energies initially stored as metastable energy and as vibrational energy.

We assume that elastic collisions between the ambient electrons are sufficiently frequent that the electron velocity distribution is Maxwellian, characterized by an electron temperature T_e . The electron gas cools by collisions with the neutral particles and positive ions, which we assume have a common temperature T_g . For the energy loss in elastic collisions with atomic oxygen we adopt the expression

$$\left(\frac{d T_e}{dt}\right)_o = - 10^{-14} n(0) T_e^{1/2} (T_e - T_g). \quad (20)$$

which corresponds to a constant collision cross section of 6×10^{-17} cm² (Rothe, Marino, Neynaber and Trujillo, 1962). For the energy loss in collisions with molecular nitrogen we use

$$\left(\frac{d T_e}{dt}\right)_{N_2} = - \left\{ 7.6 \times 10^{-16} T_e + \left(\frac{G \bar{v}}{n(N_2)}\right)_{rot} \right\} n(N_2) (T_e - T_g), \quad (21)$$

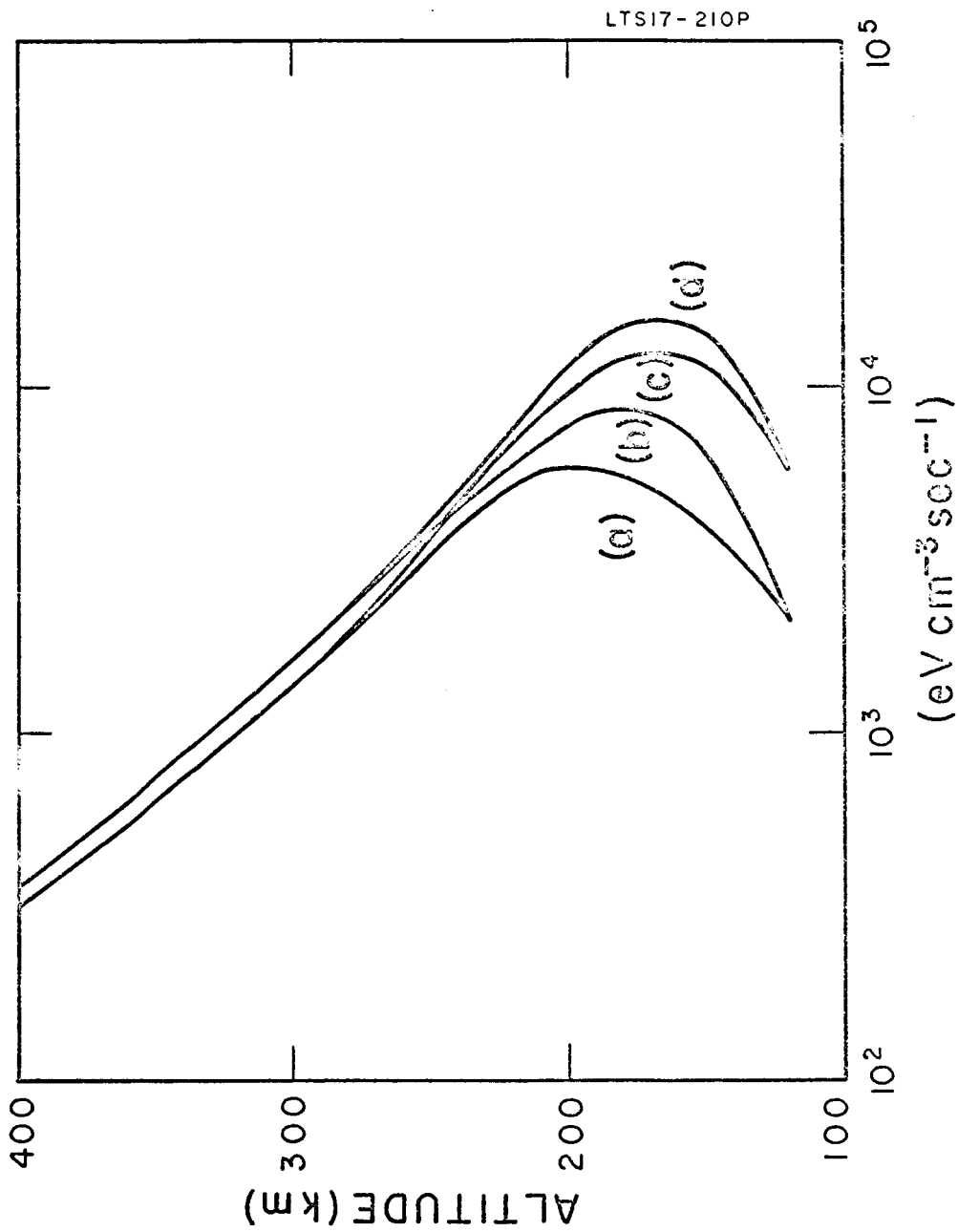


Figure 19. Heat fluxes to the ambient electrons for the atmosphere with $T(\infty) = 1000^\circ\text{K}$:
 curve (a) excluding metastable energy and excluding vibrational energy;
 curve (b) including metastable energy but excluding vibrational energy;
 curve (c) excluding metastable energy but including vibrational energy;
 curve (d) including metastable energy and including vibrational energy.

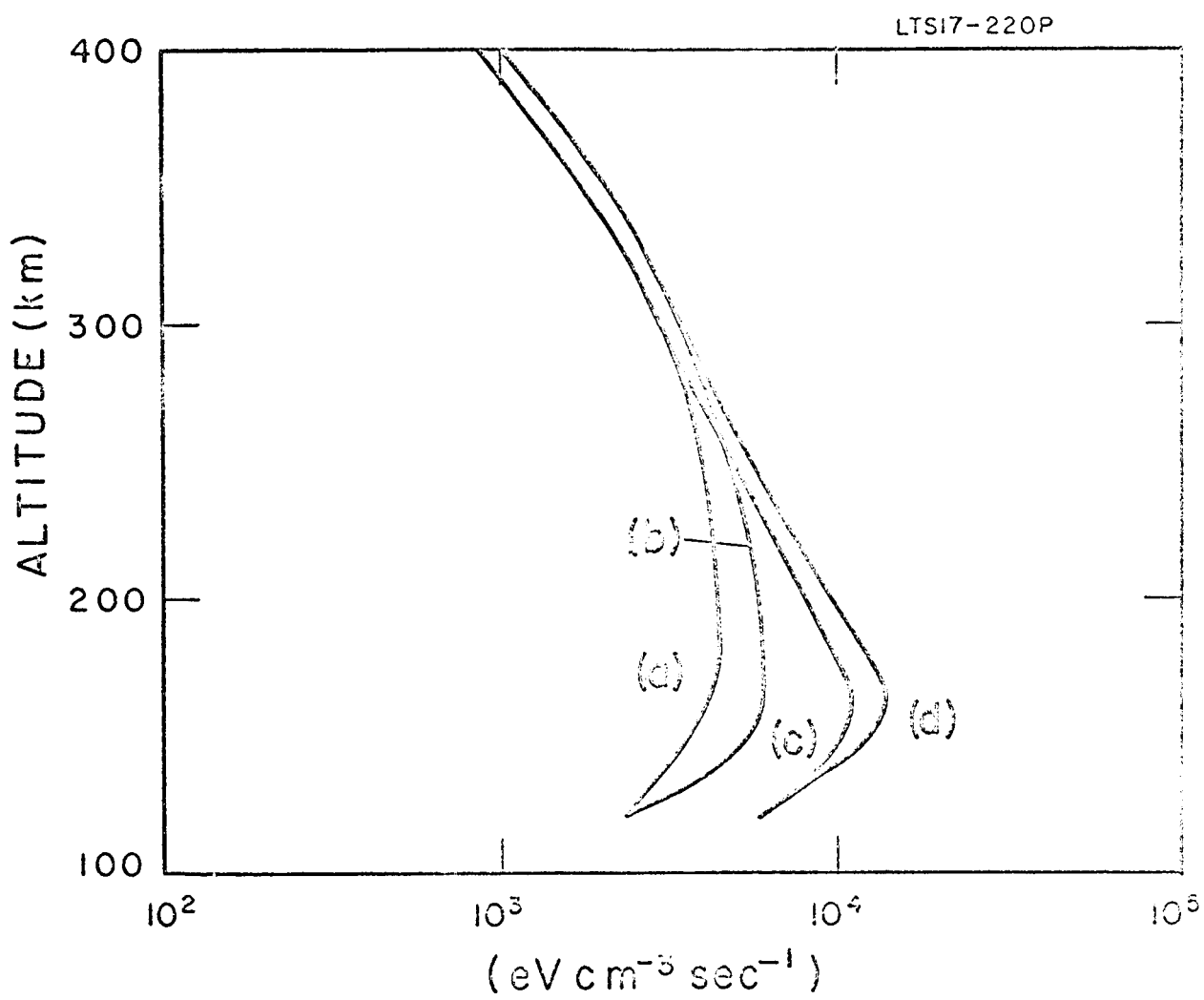


Figure 20. Heat fluxes to the ambient electrons for the atmosphere with $T(\infty) = 2000^\circ\text{K}$. The labelling of the four curves is as for Figure 19.

the elastic loss following from the measurement of Pack and Phelps (1961) and the rotational loss parameter $(Gv/n)_{rot}$ from an extension of the calculations of Dalgarno and Moffett (1962b). For loss to molecular oxygen, we use an elastic contribution only

$$\left(\frac{dT}{dt}\right)_{O_2} = -4.7 \times 10^{-16} n(O_2) Te (Te - Tg) \quad (22)$$

(cf. Dalgarno 1961). The energy loss in elastic collisions with positive ions is significant above an altitude of 200 km. At such altitudes we may suppose the positive ions are mainly O^+ and the corresponding rate of energy loss is given by

$$\left(\frac{dT}{dt}\right)_+ = -\frac{n_e (Te - Tg)}{268 Te^{3/2}} \quad (23)$$

(cf. Spitzer 1956, Hanson and Johnson 1961). If Q is the heat in ergs cm^{-3} transferred to the electron gas in unit time, then in equilibrium

$$Q = -\frac{3kn_e}{2} \left\{ \left(\frac{dT_e}{dt}\right)_0 + \left(\frac{dT_e}{dt}\right)_{N_2} + \left(\frac{dT_e}{dt}\right)_{O_2} + \left(\frac{dT_e}{dt}\right)_+ \right\} \quad (24)$$

Because it ignores the contributions from vibrational excitation, the adopted cooling rate is probably too slow at high temperatures. However, the uncertainties in the cooling rates are smaller than the uncertainties in the predicted heat fluxes.

5. Electron Temperatures

It is instructive to consider first the equation which results when cooling occurs only by elastic collisions with positive ions. If Q is measured in $\text{eV cm}^{-3} \text{ sec}^{-1}$, the simplified equation for the electron temperature is

$$Q = 5.51 \times 10^{-7} \frac{n_e^2 (T_e - T_g)}{T_e^{3/2}} \quad (25)$$

As Hanson and Johnson (1961) have remarked, (25) has two solutions for Q less than a critical value Q_{ci} but for Q greater than Q_{ci} (25) has no solutions and T_e is not limited by energy transfer to the positive ions. The critical heat input is given by

$$Q_{ci} = 2 \times 10^{-7} n_e^2 T_g^{-\frac{1}{2}} \text{ eV cm}^{-3} \text{ sec}^{-1} \quad (26)$$

and the corresponding equilibrium electron temperature is given by

$$T_e = 3 T_g \quad (27)$$

The modifications caused by the inclusion of cooling by energy transfers to the neutral particles depend upon the altitude. Below about 200 km, cooling in collisions with neutral particles is more efficient at all temperatures than cooling in collisions with positive ions and there is only one solution to (24). At greater altitudes, the

position is more complicated. Figure 21 shows the right-hand side of Equation (24) as a function of T_e at an altitude of 400 km in the atmosphere with an exospheric temperature of 1000°K . It is apparent that for heat inputs Q greater than $1.3 \times 10^4 \text{ eV cm}^{-3} \text{ sec}^{-1}$ and less than $7.8 \times 10^3 \text{ eV cm}^{-3} \text{ sec}^{-1}$ there is only one solution of (24) but that for Q lying between these values there are three solutions. Of the three solutions, the smallest and the largest are stable in the sense that after a small disturbance the departure of T_e from its equilibrium value will decay exponentially with increasing time and the remaining solution is unstable.

It is also apparent from Figure 21 that as Q passes through the value $1.3 \times 10^4 \text{ eV cm}^{-3} \text{ sec}^{-1}$ from below the equilibrium electron temperature increases discontinuously to a very large value. The opposite behaviour occurs as Q passes through the value $7.8 \times 10^3 \text{ eV cm}^{-3} \text{ sec}^{-1}$ from above.

Solutions of Equation (24) are given in Table 7 for a wide range of heat inputs, together with the critical heat inputs Q_{ci} . The equilibrium electron temperature increases very slowly as Q increases through several orders of magnitude until Q exceeds Q_{ci} when an abrupt increase in T_e occurs at high altitudes. The very large values of T_e obtained at high altitudes for Q greater than Q_{ci} do not have any quantitative significance (since at such values the adopted cooling rate is much too small and heat conduction in the electron gas is an important effect) but they show that for Q in the neighborhood of Q_{ci}

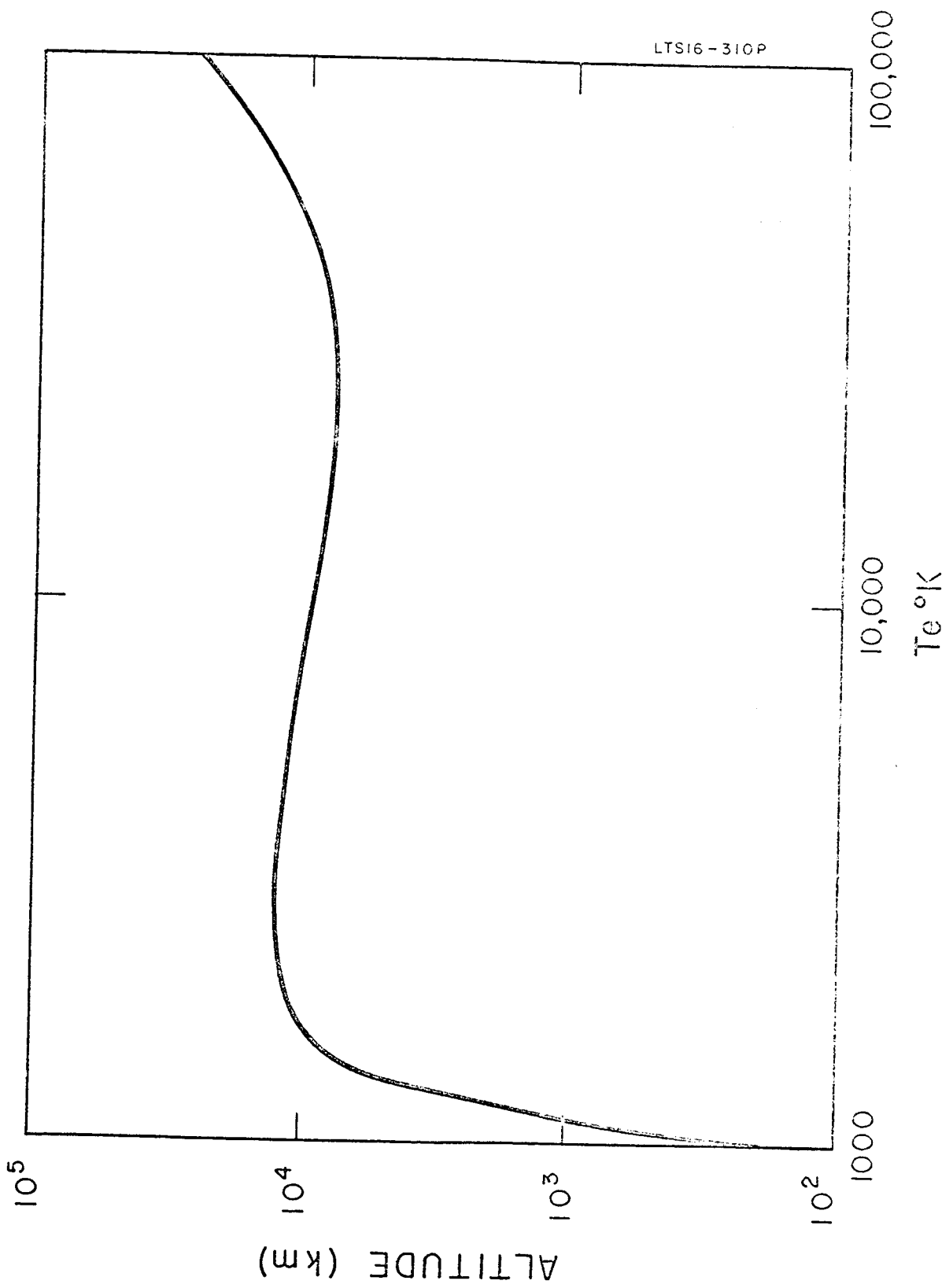


Figure 21. The right-hand side of Equation (24) as a function of Te at an altitude of 400 km in the atmosphere with $T(\infty) = 1000^\circ\text{K}$.

Table 7

Equilibrium Electron Temperatures for a Range of Heat Inputs Q

 $T(\infty) = 1000^{\circ}\text{K}$

		Altitude (km)	120	150	200	300	400	450
Q (eV $\text{cm}^{-3} \text{sec}^{-1}$)	T_g ($^{\circ}\text{K}$)	380	763	952	998	1,000	1,000	
10^1	T_e ($^{\circ}\text{K}$)	380	763	953	998	1,000	1,000	
10^2		381	767	960	1,000	1,000	1,000	
10^3		385	801	1,040	1,020	1,030	1,050	
10^4		427	1,160	2,390	1,380	1,680	132,000	
10^5		847	4,190	12,000	43,700	223,000	---	
$T(\infty) = 2000^{\circ}\text{K}$		T_g ($^{\circ}\text{K}$)	380	880	1,390	1,810	1,940	1,970
10^1	T_e ($^{\circ}\text{K}$)	380	880	1,390	1,810	1,940	1,970	
10^2		381	884	1,400	1,820	1,950	1,980	
10^3		385	924	1,510	1,870	2,030	2,100	
10^4		427	1,330	2,920	2,800	6,390	22,600	
10^5		847	4,590	11,900	24,600	64,100	103,000	

a large increase in T_e may result from a small increase in Q .

Corresponding to each of the predicted heat inputs, shown in Figures 19 and 20, there is only one possible equilibrium electron temperature and it is stable. The distributions of T_e with altitude are shown in Figures 22 and 23 from which it appears that the difference between the electron temperature and the heavy particle temperature at noon in a quiet ionosphere may attain a maximum value of between 800°K and 1500°K (depending upon the role of metastable and vibrational energy) at an altitude near 250 km and that it vanishes below about 120 km and above about 400 km. Very large values of T_e do not occur because the predicted heat inputs exceed the critical values Q_{ci} only at altitudes below about 250 km where cooling by energy transfer to neutral particles is at least comparable in efficiency at all temperatures to cooling by energy transfer to positive ions.

The predicted values are sufficiently large to suggest that the heat inputs at high altitudes might exceed the critical values near dawn and during severely disturbed conditions with the consequence that very large values of T_e may occur then, although the heating effect of the increase in Q will be reduced by the associated increase in the ambient number density. Simultaneous measurements of T_e and n_e at dawn would be of great interest.

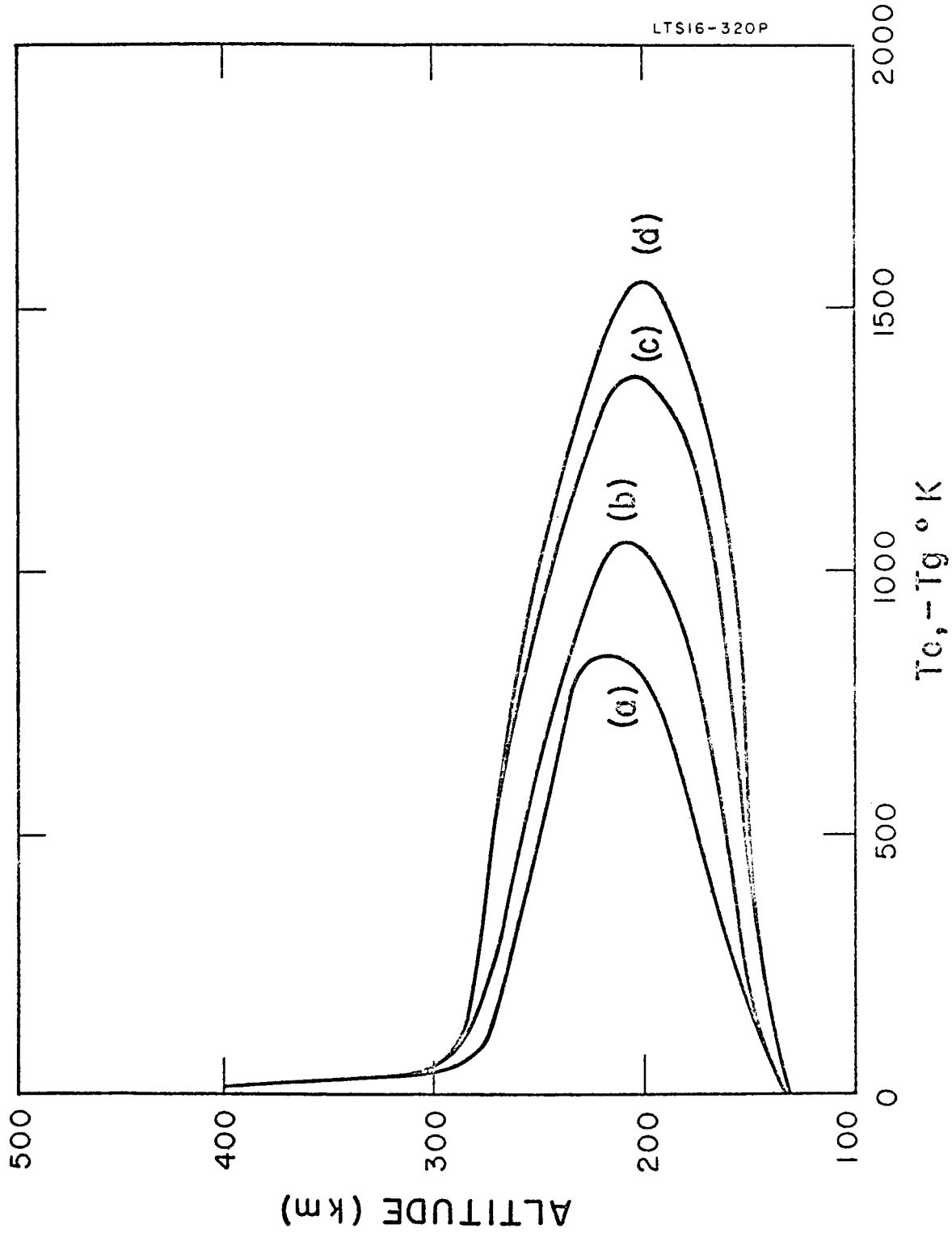


Figure 22. Electron temperatures corresponding to the heat inputs of Figure 19.

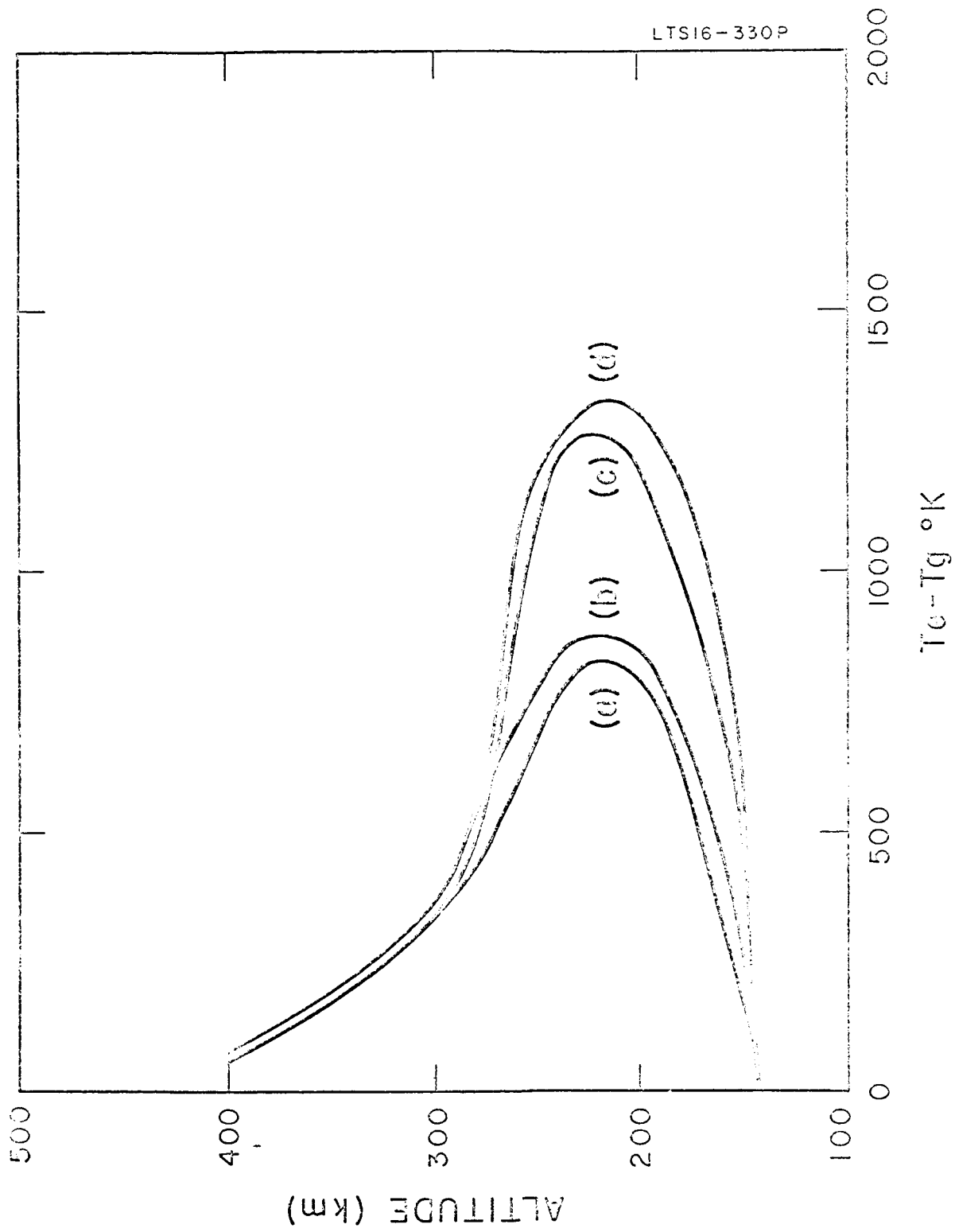


Figure 23. Electron temperatures corresponding to the heat inputs of Figure 20.

6. Discussion

The observational evidence concerning electron temperatures in the ionosphere has been reviewed recently by Bauer and Bourdeau (1962). They conclude that except at sunrise the electron and neutral particle temperatures in a quiet ionosphere are equal up to altitudes of 200 km and at altitudes above the F2 peak. In the lower F region, the difference between the electron temperature and the heavy particle temperature attains a maximum value of about 1000°K at an altitude near 250 km.

In view of the several uncertainties in the theoretical analysis, the agreement between the theoretical predictions and the observations is very satisfactory. Indeed the observed magnitude of the maximum temperature difference is closely equal to that predicted for the case when vibrational energy of molecular nitrogen is not transferred to the electron gas. The predicted location of the maximum is about 30 km lower than that observed but this small discrepancy can plausibly be attributed to an underestimate of the cooling rate, especially in view of recent work by Phelps (1962, private communication) indicating that the cross section for low energy excitation of the first vibrational level of molecular nitrogen is quite large. Thus the observational data on electron temperatures in a quiet ionosphere can be explained as due to the direct action of solar ultraviolet radiation and it is unnecessary to postulate the existence of electric fields.

At sunrise and during disturbed conditions the observational results indicate greater departures from temperature equilibrium (cf. Bauer and Bourdeau 1962) and work is in progress to analyze these phenomena.

**Geophysics Corporation of America
Bedford, Massachusetts
November 1963**

REFERENCES

- Bates, D.R., 1955, J. Atmos. and Terr. Phys., 6, 171.
- Bates, D.R., 1959, Proc. Roy. Soc., A, 253, 451.
- Bates, D.R. and Patterson, T.N.L., 1961, Planet. Space Sci., 5, 328.
- Bauer, S.J. and Bourdeau, R.E., 1962, J. Atmos. Sci., 19, 218.
- Butler, S.T., and Buckingham, M.J., 1962, Phys. Rev., 126, 1.
- Dalgarno, A., 1961, Annales de Geophys. 17, 16.
- Dalgarno, A., 1963, Planet. Space Sci. (In press).
- Dalgarno, A. and Griffing W.G., 1958, Proc. Roy. Soc. A, 248, 415.
- Dalgarno, A. and Moffett, R.J., 1962a, Proc. Nat. Acad. Sci. India (In Press). (Symposium on Collision Processes).
- Dalgarno, A. and Moffett, R.J., 1962b, Planet. Space Sci., 9, 439.
- Dalgarno, A., and Parkinson, D., 1960, J. Atmos. Terr. Phys., 18, 335.
- Fite, W. L. and Brackman, R.T., 1959, Phys. Rev. 112, 815.
- Haas, R., 1957, Zeits. f. Physik, 148, 177.
- Hanson, W.B. and Johnson, F.S., 1961, Mémoires Soc. R. Liège Serie 5, 4, 390.
- Pack, J.L., and Phelps, A.V., 1961, Phys. Rev., 121, 798.
- Ratcliffe, J.A., 1960, Physics of The Upper Atmosphere (Academic Press).
- Rothe, E.W., Marino, L.L., Neynaber, R.H., and Trujillo, S.M., 1962, Phys. Rev., 125, 582.
- Schulz, G.J., 1962, Phys. Rev., 125, 229.
- Schulz, G.J., and Dowell, J.T., 1962, Phys. Rev., 128, 174.
- Seaton, M.J., 1956, "The Airglow and The Aurorae," (Pergamon Press: London) Eds. E.B. Armstrong and A. Dalgarno.

Seaton, M.J. and Osterbrock, D.E., 1957, *Astrophys. J.*, 125, 66.

Spencer, N.W., Brace, L.H. and Carignan, G.R., 1962, *J. Geophys. Res.*, 67, 157.

Spitzer, L., 1956, *Physics of Fully Ionized Gases* (Interscience: New York).

Tate, S.H. and Smith, P.T., 1932, *Phys. Rev.* 39, 270.

Thompson, J.B., 1959, *Proc. Phys. Soc.*, 73, 831.

Watanabe, K., and Hinteregger, H.E., 1962, *J. Geophys. Res.*, 67, 999.